

AD A 045121

10

B S.

**DYNAMIC IMPACT RESPONSE BEHAVIOR
OF POLYMERIC MATERIALS**

FINAL REPORT

(1 May 1976 to 30 April 1977)

August 1977

D D C
RECEIVED
OCT 11 1977
LIBRARY
C

Prepared Under Contract N00019-73-C-0330

For

**Naval Air Systems Command
Department of the Navy
Washington, D. C. 20361**

By

**Corporate Research and Development
General Electric Company
Schenectady, N. Y. 12301**

FILE COPY

APPROVED FOR PUBLIC RELEASE; DISTRIBUTION UNLIMITED

Unclassified

SECURITY CLASSIFICATION OF THIS PAGE (When Data Entered)

REPORT DOCUMENTATION PAGE

READ INSTRUCTIONS BEFORE COMPLETING FORM

1. REPORT NUMBER	2. GOVT ACCESSION NO.	3. RECIPIENT'S CATALOG NUMBER
------------------	-----------------------	-------------------------------

4. TITLE (and Subtitle) Dynamic Impact Response Behavior of Polymeric Materials,	5. TYPE OF REPORT & PERIOD COVERED Final Report, 26 May 76 to 27 Apr 77
--	---

7. AUTHOR(s) William B. Hillig	6. PERFORMING ORG. REPORT NUMBER 1 May 76 - 30 Apr 77
--	---

9. PERFORMING ORGANIZATION NAME AND ADDRESS General Electric Company Corporate Research and Development P.O. Box 8, Schenectady, NY 12301	10. PROGRAM ELEMENT, PROJECT, TASK AREA & WORK UNIT NUMBERS
---	---

11. CONTROLLING OFFICE NAME AND ADDRESS Naval Air Systems Command Department of the Navy Washington, DC 20361	12. REPORT DATE August 1977
---	---------------------------------------

14. MONITORING AGENCY NAME & ADDRESS (if different from Controlling Office) 1278p.	13. NUMBER OF PAGES 77
--	----------------------------------

15. SECURITY CLASS. (of this report) Unclassified
15a. DECLASSIFICATION/DOWNGRADING SCHEDULE

16. DISTRIBUTION STATEMENT (of this Report)
Approved for public release; distribution unlimited.

17. DISTRIBUTION STATEMENT (of the abstract entered in Block 20, if different from Report)

18. SUPPLEMENTARY NOTES

19. KEY WORDS (Continue on reverse side if necessary and identify by block number)
**Hopkinson Bar
Ballistic Impact
Impact Damage of Polymers**

20. ABSTRACT (Continue on reverse side if necessary and identify by block number)
The work reported was devoted to making reliable, quantitative impact pulse measurements for free-flight encounters between a spherical projectile and the desired target material. This effort builds on, but also contrasts with, previous studies which involved indentations at programmed incursion rates. Because of the change of techniques involved, developing and verifying the associated instrumented and computation systems were a major part of the effort. The materials of interest continue to be polycarbonate PC, poly-

117

Methylmethacrylate PMMA, and epoxy resins. Inorganic glass was also used as a target material because impacts can be confidently modeled from theory in this case.

Impact pulse determinations were made on the four target materials with hardened steel strikers of 4.5 mm diameter tips weighing 42 g and of 19 mm diameter weighing 28.3 g usually at 2.5 m per second. The impact strain pulse shapes are increasingly narrower and higher peaked in the order PC, epoxy, PMMA, glass. Semi-quantitative analysis of the general shapes indicates little irreversible deformation work is performed during impacts involving 19 mm striker. However, using the 4.5 mm striker causes irreversible absorption of the net energy received from the striker. The fractional amount absorbed in this series of measurements decreased in the order PC, epoxy, PMMA, and glass.

Computer procedures were developed for analyzing and correcting the detailed pulse shapes to reveal how the force and penetration are related and to follow the evolution of the various energy and momentum contributions. The computer procedures have been verified by using as input model impact pulses, calculated from Hertz elastic theory. However, when the experimentally observed pulse shapes are used as input, the computed force versus penetration behavior is at variance with expectation. Distortion of pulse shape as it travels down the bar is suggested as being responsible. Candidate procedures for dealing with this problem are outlined, additional possible factors are offered, and the implications for future work at greater impact velocities are discussed.

Administrative stamp with fields for 'BY', 'DATE', and 'DISTRIBUTION/AVAILABILITY CODES'. Includes a handwritten signature 'A' and a checkmark.

TABLE OF CONTENTS

	Page
SUMMARY	v
1. INTRODUCTION	1-1
1.1 Prior Work	1-2
1.2 Present Objectives	1-6
2. MATERIALS AND SPECIMEN PREPARATION	2-1
2.1 Polymethylmethacrylate	2-1
2.2 Polycarbonate	2-1
2.3 Epoxy	2-1
2.4 Inorganic Glass	2-1
3. IMPACT MEASUREMENTS	3-1
3.1 Impact Apparatus	3-1
3.1.1 The Impact Bar	3-1
3.1.2 Striker	3-3
3.1.3 Electronic Instrumentation	3-5
3.2 Experimental Procedure	3-6
3.3 Auxiliary Measurements	3-6
3.4 Experimental Impact Results	3-7
4. ANALYSIS OF DATA	4-1
4.1 Basic Equations	4-1
4.2 Integration Procedures	4-4
4.3 Momentum Measurements	4-5
4.4 Correction for Post-Pulse Behavior	4-7
4.5 Studies Using Inorganic Glass Targets	4-9
4.5.1 Theoretical Elastic Impact Pulse	4-10
4.5.2 Critical Experiments	4-11
4.5.3 Preliminary Fourier Analysis	4-14
4.6 Treatment of Pulse Data	4-16
4.6.1 Detailed Kinematic Analysis	4-16
4.6.2 Macro Kinematic Analysis	4-18
5. DISCUSSION	5-1
6. ACKNOWLEDGMENT	6-1
7. REFERENCES	7-1
FIGURES	following 7-1

SUMMARY

This report covers the work done during the twelve-month period beginning May 1976 and is devoted to making reliable, quantitative impact pulse measurements for free-flight encounters between a spherical projectile and the desired target material. This work builds on, but also contrasts with, previous studies which involved indentations at programmed incursion rates. Because of the change of techniques involved, developing and verifying the associated instrumented and computation systems were a major part of the effort. The materials of interest continue to be polycarbonate PC, polymethylmethacrylate PMMA, and epoxy resins. Inorganic glass was also used as a target material because impacts can be confidently modeled from theory in this case.

The experimental procedure involves mounting the specimen on a long PMMA impact bar, which is free to swing in a pendulum-like manner. A striker of desired mass and geometry is similarly arranged to allow an impact with the specimen at a known impact velocity at a controllable spot on the specimen. Momentum change measurements are made, and the strain pulse as it travels down the bar is sensed by a strain gage suitably amplified and recorded. The system was calibrated so as to relate the output signal to the force on the bar.

Impact pulse determinations were made on the four target materials with hardened steel strikers of 4.5 mm diameter tips weighing 42 g and of 19 mm diameter weighing 28.3 g usually at 2.5 m per second. The general pulse shapes are increasingly narrower and higher peaked in the order PC, epoxy, PMMA, glass. A semi-quantitative analysis of the general shape parameters suggests there is little irreversible energy of deformation occurring during any of the impacts involving the 19 mm striker,

but that 25% of the net energy imparted to PC using the 4.5 mm striker was irreversibly absorbed. The fractional amount absorbed in this series of measurements decreased in the order PC, epoxy, PMMA, and glass. The value for the latter is postulated as being zero.

Computer procedures were developed for analyzing and correcting the detailed pulse shapes to reveal how the force and penetration are related and to follow the evolution of the various energy and momentum contributions. These analyses are based on the somewhat simplified assumption that the pulse is uniform over the cross section of the bar. The computer procedures have been verified by using as input model impact pulses calculated from Hertz elastic theory. However, when the experimentally observed pulse shapes are used as input, the computed force versus penetration behavior is at variance with expectation. Distortion of pulse shape as it travels down the bar is suggested as being responsible. Candidate procedures for dealing with this problem are outlined, additional possible factors are offered, and the implications for future work at greater impact velocities are discussed.

DYNAMIC IMPACT RESPONSE BEHAVIOR OF POLYMERIC MATERIALS

1. INTRODUCTION

The response of polymers to impact from small, hard bodies has a wide range of technical and practical implications. As stated in our previous reports, such a seemingly simple event in fact involves a number of scientifically distinctly different but coupled phenomena. The sorting out and determination of the separate phenomena has been a non-trivial exercise. The understanding and quantification of the various processes should provide a basis for (1) achieving better impact resistance and impact resistant materials on a rational basis, (2) diagnosing impact failures and effects, and (3) characterizing and ranking materials.

The present report covers the work done during the twelve-month period beginning May 1976 and continues to focus on polycarbonate PC, polymethylmethacrylate PMMA, and epoxy resins. The work was devoted predominantly to developing and verifying the instrumentational and computational systems and to making measurements on specimens subjected to a free-flight encounter by a spherical striker. The materials of investigation were attached to the ends of an instrumented Hopkinson bar. For this purpose, measurements and calculations of the impact process using inorganic glass were undertaken. This has proven to be valuable in terms of providing insight and a rigorous test of the entire experimental/analytical approach. This year's work contrasts from that performed in prior years. Previously the penetrating body was fixed to the movable member of a mechanical test machine. That arrangement allowed the penetration velocity to be held constant or programmed in an independently controlled manner. The present work departs

from the past, both in respect to the instrumentation and the kinds of experiments performed. However, impact velocities in this study were selected to overlap with those used with the mechanical test machines to allow a direct comparison between the two methods.

The present work rests heavily on the results of the four previous yearly programs⁽¹⁻⁴⁾. Therefore, this background, especially as it provides perspective to the present effort, will be summarized. The remainder of this report will describe the impact apparatus, present the impact data obtained to date, outline the analytical computer procedures developed to translate the strain pulse impact data into reaction force-penetration information, and finally discuss the results and required future effort. Some portions of the test, e.g., background, description of materials, even though previously reported, but which are needed for completeness, will be incorporated into the present report.

1.1 Prior Work

The sustaining focus of the work has been to understand in depth the processes that occur at the collision site between the polymer of interest and the colliding object. Because there is a large body of information available on the physico-mechanical behavior of PC and PMMA, the approach was to make as much use of this scientific background as possible. Therefore, measurements were initially made at small, constant velocities using mechanical test machines. This work showed that the materials did not behave in the expected classical viscoelastic manner. This rendered some of the analytical structure that we developed inappropriate for treating the experimental results. The observed response of the polymers, even at the smallest detectable penetration depths, exhibited an unexpected form of relaxation behavior. This was coupled with an anelastic yield response mode of significant magnitude.

The yield phenomena, which are revealed from examination of the force-penetration mechanical information, appear to be associated with the development of a lens-like zone of visibly altered material under the contact site. The growth of this "disturbed" zone under the indentation was followed in PC using motion pictures. The zone was found to form virtually from the first moment of contact. The evolution of the zone geometry was quantitatively determined from the photographs. The volume of the zone is about 6 ± 1 times the volume displaced by the indenter. By assuming that the material transformation is describable as an ideal plastic yield process, the (anelastic) yield stress could be estimated using this plus other observations. Two qualitatively different estimates indicate that the yield stress in PC is between 9 and 29 ksi. The term anelastic is used because the disturbed zone and the permanent deformation anneal out completely when the polymer is heated to its glass transition temperature. These somewhat pioneering aspects of the work are expected to be relevant to other processes, such as the forming of polymer shapes, cold flow processing, and concentrated compressive loading of structural polymers.

Because classical viscoelastic theory was found to be inadequate, it was necessary to develop an extensive data base, and measurements of force versus penetration depths have been obtained at velocities ranging from 0.0002 to 6000 inches per minute. A 4.5 mm diameter ball bearing (0.177 inches) has served as the standard size indenter or projectile. However, balls two and four times as large have also been used, as well as cones of various apex angles. The data for PC and PMMA have been found to be representable by a phenomenological "equation of state" for the force F having the form

$$F = Av^n x^m$$

where v and x are indentation velocity and depth, and A , n , and m are experimentally determined constants.

Considerable attention has been given to understanding the force penetration behavior. For fixed velocity laws of the form $F = Cx^m R^\alpha$ have been proposed to describe the force F behavior in terms of the diameter of the indenter R and the penetration depth x . The other terms are characteristic constants. When the material is ideally elastic, $C = (4/3)E/(1-\gamma^2)$, where E is the Young's modulus and γ the Poisson ratio of the material; the values of α and m are $1/2$ and $3/2$ in this case, respectively. This is the behavior we expected in polymers at large indentation velocities and/or at small indentation depths. The response at high velocities up to or exceeding 300 m per second is a long-range experimental program goal. The work has focused on getting information in the regimes at which elastic behavior is expected as a reference against which actual behavior can be compared. However, no unambiguously elastic regimes were found. Furthermore, on dimensional grounds $(\alpha + m)$ should equal two. However, this value was generally not observed, implying that additional factors are involved in the impact process. It has become increasingly evident that time variations in velocity have a large effect on the response behavior.

At first glance this conclusion appears to be at variance with the observations made under conditions of constant velocity in which the force required to drive an indenter into the polymer was found to be relatively insensitive to the rate of indentation over a span of $7\ 1/2$ decades of the velocity. However, the reason was not that the apparent elastic modulus was so insensitive to rate, but was due rather to the surprisingly strong dependence of the characteristic stress relaxation time on the prior indentation velocity. At high velocities, the relaxation time was short, whereas at low velocities the relaxation time was long. As a result of these compensating factors for a given penetration depth, the force developed while the indenter is moving is only weakly dependent on velocity.

The pronounced effect of time dependence is revealed most vividly under conditions in which the rate of incursion is abruptly changed or reduced to zero. Such work was done in

detail on PC and PMMA as a part of Contract N00019-75-C-0320 under a broad range of conditions. Pronounced hardening of the material was noted when the material was allowed to rest after having been deformed. That is, the compliance was markedly reduced on restarting the incursion process, after having stopped it temporarily, relative to what it would be if it had not been stopped. These measurements were made as a function of halt duration to determine the effect of history on the material response. Similar measurements were made over a range of depths to define how the relaxation process varies with deformation. Complementary studies were made of the creep recovery of the deformation crater as a function of time under several sets of conditions. These combined results provide a relatively complete picture of the relaxation responses over a broad range of conditions. Applying this information to PC and PMMA, it was possible to correct the observed curves of the force versus depth for relaxation effects. This results in the establishment of the "instantaneous" response curve for these materials, i.e., the inferred response if the material could be deformed infinitely fast.

The load relaxation upon halting the indentation was found to be given over a wide range of times by the unusual equation

$$F(t) = F(o) (1 + At)^{-B}$$

where $F(t)$ is load at time t after stopping the indenter, $F(o)$ is the load at the instant of stop, and A and B are experimental constants. The constant A is strongly dependent on the indentation rate, and the second constant B being much less dependent. For the polymer to respond quasi-elastically, no relaxation must occur during the period of loading. This means that the product AB must become zero. Over the velocity regime explored to date, there is no clear evidence when this will occur. A relatively simple molecular model was formulated which "predicts" the

identical stress relaxation law which had been empirically found to provide the best fit of the relaxation data. The model also predicts the experimentally found proportionality between the constant A and the penetration rate (prior to stopping the indenter). However, further work is needed to test the validity of the model under other sets of conditions, such as sinusoidal loading, free impact, etc.

Although the use of mechanical test machines is convenient, indentations in which velocity is held constant independent of depth do not correspond to the physical event of a free impact. During a collision between a (rigid) projectile and the polymer target material (free impact), the projectile velocity constantly decreases because the indentation forces decelerate the projectile, i.e., the velocity is an implicitly determined variable. Thus, determining the force-time penetration response when the velocity was varied in an independently controlled manner, was undertaken as a problem of intermediate level of complexity. Data on PC and PMMA were obtained for several incursion amplitudes and periods. The above "equation" of state" was partially successful in describing the response.

The work just described sets the stage for undertaking the next level of complexity, viz., determining, analyzing, and finally predicting the response due to free-impact encounters up to velocities of about 300 m per second. Preliminary work showed that in principle an instrumented ballistic impact bar could be used to make the required observations, but that there would be substantial experimental, instrumental, computational, and conceptual challenges in quantitatively bridging the gap between the mechanical test machine work of the past and the ballistic impact work.

1.2 Present Objectives

The original objectives set forth in the work statement were (1) to measure the impact response from a 4.5 mm diameter steel

projectile over the velocity range of 100 to 1000 feet per second, (2) to measure the response when mass, diameter, or other shape variables are altered, (3) to obtain cinematographic records of impact testing for use in qualitative and quantitative interpretation, and (4) to develop further theoretical and analytical models of impact behavior to further define the basic constituent physical processes.

During the pursuit of the work, it became clear that the tasks of developing the instrumentation, detecting, processing, and understanding of the results would be more demanding than originally expected. Accordingly, whereas the objectives given above provided the long-term framework, the work can better be described in terms of the following nearer-term goals:

(1) Set up an instrumented Hopkinson bar impact apparatus and demonstrate its capability for detecting the impact pulse with sufficient resolution and accuracy to permit analysis of the data which can provide continuity with the previous work.

(2) Calibrate and establish the reliability of the impact apparatus.

(3) Obtain stress pulses in which the radius, mass, and velocity of the projectile are varied using PC, PMMA, and epoxy as the target materials.

(4) Provide velocity overlap between the upper end of the mechanical test machine experiments and the lower end of the gas gun capability.

(5) Develop the computer software needed to translate the observed stress pulse into force, penetration, energy, momentum transfer, and other related information.

(6) Develop further and critically analyze theoretical models which can permit calculation of the force produced under conditions of varying velocity.

The details of this work are presented in Sections 3 and 4.

2. MATERIALS AND SPECIMEN PREPARATION

The PC and PMMA materials were unchanged from those used in the previous study. Specimens were used as cut out of sheet stock, making sure that all burrs were removed. The standard specimen size was 1 x 1 x 0.5 inches. The other target materials are described below.

2.1 Polymethylmethacrylate

Specimens were cut from a single sheet of Type G Plexiglas[®] PMMA (produced by Rohm and Haas). Continuing with our former practice, the sheet was marked off in squares for cutting and a record kept so that the original location of each specimen in the sheet could be identified.

2.2 Polycarbonate

The PC resin was manufactured by the General Electric Company and is designated as Lexan[®] resin general purpose glazing sheet, Type 9034-112. A single sheet of 0.5 inch thick material was used, and specimens marked, and records kept as for the case of PMMA.

2.3 Epoxy

The epoxy specimens were of previous stock which was molded out of a mixture of 20% by weight of methylene dianiline with Epon[®] 828 resin manufactured by Shell Chemical Co. Resin was cut into a 0.5 inch slab, cured, and cut into 1.0 x 1.0 inch samples.

2.4 Inorganic Glass

Two types of samples were used having different compositions. One type was a Pyrex glass cut and ground into 0.5 x 1.0 x 1.0 inch samples. The other type was a soda lime glass cut into 0.75 x 0.75 inch samples from sheets 0.022 inches thick.

3. IMPACT MEASUREMENTS

This section describes the development of the impact bar apparatus, the various critical components, and the experimental procedure for making the impact observations. This is followed by a description of required certain auxiliary measurements, and finally by a presentation of the stress pulses obtained on PC, PMMA, epoxy, and glass under several conditions.

3.1 Impact Apparatus

The overall apparatus is shown schematically in Fig. A. The detailed descriptions of the various components follow.

3.1.1 The Impact Bar. Conventionally the materials to be studied under impact, using the instrumented Hopkinson bar technique, are made into a bar. The end is struck by a projectile, and the stress (or strain) pulse detected at some position along its length by a suitable sensor. The motion of the bar is used to measure the momentum transfer.

However, in our work we wish to examine a number of materials under a variety of conditions. Therefore, our plan has been to mount specimens of the materials of interest onto the end of a given impact bar. The samples are held in place by a viscous acoustic coupling substance, which also facilitates the transfer of the pulse generated by the impact to the bar.

In order to minimize any problems due to acoustic impedance mismatch that could cause the signal to be reflected at the specimen/bar interface, the bar material was chosen to be PMMA. The acoustic impedance is given by $\sqrt{E\rho}$, where E is the Young's modulus and ρ is density. Since the densities of polymers are nearly constant and since the moduli vary within a factor of about two for the polymers of present interest, the impedances are relatively well matched. This would not be the case if the bar were metal or glass. A further

advantage of using PMMA for the bar is its relatively small value for E. Hence, a correspondingly large strain is developed for a given magnitude of stress. Since a strain gage is used to detect the pulse, less signal amplification is needed, with benefits for the signal-to-noise ratio.

Preliminary measurements indicated that the expected stress pulse duration would be 500 microseconds in length. Since the sound velocity in PMMA is about 2000 m per second, a bar length of at least 1 m is indicated. A bar of about twice this length was selected.

The bar has a square 0.75 x 0.75 inch (19 mm x 19 mm) cross section, is 72 inches (1.83 m) long, and weighs about 800 g. Two SR-4[®] strain gages are mounted on opposite sides of the bar, about 30 cm from the struck end so as to compensate for possible bar bending due to the impact. A planar horizontal support is provided overhead. This provides a base for attaching fine strings which support the impact bar and the striker in such a way as to permit pendulum swinging motion to occur in the direction of the long axis of the bar. Side-wise motion is prevented by use of a bifilar, V-shaped arrangement in which the bar and also the striker are attached to the apex, and the ends of the arms are attached to the overhead support. The plane of the V is oriented perpendicularly to the long axis of the bar, preventing transverse motion. By adjusting the strings, the position of the bar is fixed, except for the degree of freedom of motion along its long axis. The bar is suspended 108 cm beneath the overhead support.

The strain gages are embedded in the bar about 2 mm deep, and the necessary electrical leads follow the string supports so as not to interfere with the free swing of the bar. It was found that orienting the strain gages so that they were on the sides of the bar, and not on the top and bottom, was preferable. The reason was that some gravitational bending of the bar was unavoidable, so that some excitation of bending modes in the

vertical plane always occurred. Even so, some horizontal bending or buckling modes were excited. It was, therefore, found to be beneficial to locate the strain gages at a nodal position for this motion, which was located at one-sixth of the bar length. The strain gage and support arrangement is shown in Fig. A, and the effect of moving the gages from an anti-node to a node position is shown in Figs. B and C.

As a means of measuring the motion of the bar caused by the impact, a rider traveling along a taut wire is moved by a metal finger attached to the bar. A steel ruler is mounted behind the wire for convenience in determining the change in position of the rider. This is the quantity D_{bar} shown in Fig. 3.1A.

3.1.2 Striker. The projectile (striker) was attached to the end of a single bifilar, V-shaped string support, as described in 3.1.1 for the case of the impact bar. By careful location of the upper attachment eyes and adjustment of the two legs of the "V," the impacter could be made to strike the specimen target reproducibly on the longitudinal axis of symmetry of the bar. Different strikers were used. In the case of 12.7 and 19 mm diameter steel ball bearing strikers, the mass was adequate to produce a substantial impact with an approximately 250 cm per second impact. This was produced by allowing the striker to drop about 30 cm from its starting height, shown as H_{ball} in Fig. 3.1A. As noted in our previous work and when using the gas gun, 4.5 and 9 mm (2.25 and 4.5 mm radii of curvature) diameter projectiles have been standard in our work. Thus, short (ca. 7.5 cm), threaded, hardened steel bars were made, and the ends ground to these radii of curvature. Five threaded attachable masses of 7 g each could be screwed onto the strikers. In this way momenta corresponding to velocities of about 60, 120, 180, 240, and 300 m per second can be imparted to the striker using the standard pendulum geometry. These bar-shaped strikers were fitted with two

bifilar supports to ensure that the striker remained aligned, with its long axis coinciding with that of the impact bar, as well as possible.

The striker was held in the poised position, ready to be released for impact by means of an electromagnet. This facilitated easy measurement of its initial position. A metric ruler positioned along the path of the striker trajectory, along with a camera, positioned for minimum parallax error was used to measure the recoil, D_{ball} in Fig. 3.1A, of the striker. A cathetometer was provided to measure the height of the striker in its initial and contacting positions.

3.1.3 Electronic Instrumentation. The instrumentation consisted of (1) a strain gage bridge and power supply, (2) a differential amplifier linear to frequencies in excess of 1 MHz to amplify the strain gage signal prior to introducing it to the storage oscilloscope, (3) a digital storage oscilloscope to detect and store the pulse allowing it to be recorded later at slower speed, and (4) a time-base strip chart recorder. These units are described more fully next.

(1) The SR-4[®] strain gages are of type FAE-25-12S6EL with a gage factor (i.e., relative change in resistance per unit strain) of $2.06 \pm 1\%$. Each gage had a resistance of 120.0 ± 0.2 ohms. Two strain gages were located in non-adjacent arms of a conventional Wheatstone bridge circuit.

(2) The strain gage conditioning unit was a Daytronics package comprised of a 9005 main frame power supply and a 9171 strain gage conditioner. This unit provided a stabilized, filtered 5 volt DC excitation voltage to the bridge.

(3) A Tektronix differential amplifier model 5A22N was used to amplify the strain gage signal with as little distortion as possible. The bandwidth for this amplifier ranges from DC to 1 MHz and the input impedance is 1 megohm. A fixed gain of about 250 was maintained with a maximum common mode rejection ratio of 100,000:1.

(4) Data accumulation was performed by means of a Nicolet 1090A Explorer digital oscilloscope. This instrument has the capability of detecting and storing up to 4096 12-bit data entries at intervals as close as 1 μ sec. Plug-in differential amplifiers, 93A type D, were used to ensure a broad frequency response from DC to 5 MHz. The input impedance is 1 megohm and the common mode rejection ratio is 2500:1.

(5) Permanent data storage was achieved by recording the information gathered by the preceding instrument onto a high impedance Huston Omniscrite[®] strip chart recorder. This permitted data to be recorded such that the full scale of the paper, 10 inches, corresponds to the full scale on the oscilloscope, and 1 inch on the time base represents 160 μ sec.

3.2 Experimental Procedure

The impact experiments in broad outline involve:

(1) Attaching the specimen to the end of the bar using Dow resin 276-V9 to provide acoustic coupling. Visual inspection is made to ensure good overall contact, centering of the specimen relative to the bar and alignment of the bar and striker.

(2) Deducing the initial impact velocity of the striker from its initial height above the point where it contacts the bar, correcting for damping in the pendulum motion.

(3) Determining the recoil of the striker by a similar procedure.

(4) Deducing the recoil velocity of the impact bar from its maximum travel, correcting for frictional effects in the motion of the rider (see 3.1.1).

(5) Measurement of the various masses, permitting a macroscopic test of conservation of momentum to be made.

(6) Initial adjustment of the balance and voltage applied to the strain gage bridge circuit.

(7) Adjustment of the digital storage oscilloscope to ensure proper triggering and suitable time and signal level scale.

(8) Transfer of information from the oscilloscope, after the impact event is recorded and detected, to a strip chart recorder for a permanent record.

(9) Recording, point by point, in some cases of the initial parts of the impact pulse after contact has just been made by the striker. The oscilloscope permits digitized visual readout of the detected signal at 1 microsecond intervals.

(10) Reading the strip chart information by means of a digitizer to translate it into numerical data for computer processing.

3.3 Auxiliary Measurements

For carrying out the computations to be described in Section 4, it is necessary to know the velocity of sound in the impact bar and to have a calibration of the strain gages.

The sound velocity is conveniently measured by simply noting the time t between the passage of the maximum in the initial compressive impact pulse and its reflection as a corresponding tensile pulse. The velocity is thus simply $2L/t$, where L is the distance from the strain gage to the reflecting end of the impact bar. The observed value was 2095 m per second.

Calibration of the strain gage was accomplished by first determining the (long-term) Young's modulus of the bar. Then by dead-loading the bar compressively in the axial direction, the imposed strain is computed from the modulus, load, and bar cross section. This is then compared with the strain signal detected at the storage oscilloscope.

The long-term modulus was determined by bending the bar transversely using known loads, noting the deflection, and calculating the Young's modulus from the well-known beam bending formulas. The measured value was 3.13×10^{10} dynes/cm².

The strain gage signal was found to be linear with the applied load within experimental error over the explored strain

range, i.e., up to 20×10^{-5} cm/cm. This procedure provided a direct means for relating the strain to the oscilloscope output display. This observed calibration factor was 4.29×10^{-7} cm/cm per mV at the oscilloscope for the set of instrument settings held fixed during all measurements.

3.4 Experimental Impact Results

Impact measurements were made on Pyrex glass, PC, PMMA, and epoxy targets using 4.5 and 19 mm diameter strikers weighing 42.0 and 28.3 g, respectively. Systematic measurements at this time were made in at least duplicate and, in some cases, triplicate. In all cases except when impacting glass with the 19 mm steel ball, a nominal impact velocity of 2.5 m per second was selected. A lesser velocity of 1.7 m per second was used with the glass to avoid cracking the specimen target.

Representative impact pulses as recorded directly on the strip chart are presented in Figs. A to H. In addition, the average pulse shape parameters are given in Table A. Note that the momentum is proportional to the pulse area. It can be seen that the momentum transferred to the glass was markedly less in the case of the 4.5 mm impact on glass than when the polymers were struck. The broadest pulse occurred using PC, followed by epoxy, and PMMA as measured by any of the peak shape parameters, i.e., time for the peak maximum to occur, time breadth of peak at half maximum strain, total duration of pulse, or momentum. The maximum strains rank in the reverse order. To show typical reproducibility, an example of replicate results is shown superimposed in Fig. G for PMMA. The curves nearly coincide except for small departures at the leading and trailing portions.

As can be seen in the figures, the trailing portions of the pulses often appear to be somewhat oscillatory. The reason for this is not completely determined at this time. This may be due to excitation of bending modes, if the impact is not exactly on center, or may be due to surface waves resulting from Poisson lateral deformations.

These post-pulse waves will probably become more severe problems as the impact velocity is increased. This can be seen from the pulse shown in Fig. I obtained when a PMMA target was struck at about 100 m per second by a 4.5 mm ball shot from a compressed air gun. No attempt has been made to analyze this complex pulse at this time. Analysis of the pulses in terms of the underlying phenomenological physical processes is discussed in Section 4.

TABLE 3.4 A
Experimental Average Pulse Shape Parameters

MATERIAL	GLASS		PC		PMMA		EPOXY	
Striker Diameter* mm	4.5	19	4.5	19	4.5	19	4.5	19
Initial Impact Velocity, cm/sec	245	174	251	256	248	258	250	260
Maximum Strain $\times 10^4$	6.9	5.2	3.5	4.4	4.5	5.5	3.9	4.8
Time to Maximum μ sec	82	52	197	108	142	83	175	103
Pulse Duration μ sec	352	283	499	354	425	347	474	360
Pulse Time Width at Half Peak Height μ sec	93	53	243	141	178	102	217	124
Momentum, g cm/sec	11303	5344	14276	10409	13411	9466	14119	10059

*Mass of 19 mm striker = 28.3 g
 " " 4.5 mm " = 42.0 g

3-9

4. ANALYSIS OF DATA

4.1 Basic Equations

The basis for deducing the force indentation response in the impact event from the impact pulse was discussed in Section 6.5 of the previous report ⁽⁴⁾ and is incorporated here with minor revision for convenience.

Because the impact occurs over a concentrated area, the compressive acoustic pulse radiates initially as a spherical wave. However, as it travels down the bar, the compressive wave becomes increasingly planar. If the initial impact does not occur on the axis of symmetry of the bar, then flexural modes can be excited in the bar. Furthermore, surface and transverse waves can be expected as well. Thus, the signal detected at the strain gage comprises a complex superposition of waves. In spite of this, the data will be treated as if the strain pulse consisted only of the planar compressive component. This means the analysis will be somewhat in error and that calibration to provide the necessary corrections would be desirable.

For purposes of analysis, it is convenient to refer to the position of the struck end of the bar as the origin of the z axis and the time $t = 0$ as the instant of first contact between the ball and the bar. The ball has a mass m and is assumed to be incompressible.

Deceleration of the spherical projectile results from the local opposing material reaction force which in turn is supported elastically in the impact bar. Hence, the instantaneous deceleration force is $A\sigma(t)$ where A is the cross section of the bar, and σ the area-averaged longitudinal stress. Therefore,

$$m\ddot{z} = - A\sigma(t) \qquad \text{Eq. (a)}$$

$$= - AE\epsilon(t) \qquad \text{Eq. (b)}$$

This can be integrated directly to give

$$\dot{z} = - (AE/m) \int_0^t \epsilon dt + v_0 \quad , \quad \text{Eq. (c)}$$

and

$$z = v_0 t - \frac{AE}{m} \int_0^t \int_0^{t'} \epsilon dt' dt \quad \text{Eq. (d)}$$

where E is the Young's modulus of the bar, ϵ is strain, and v_0 is the initial velocity of the projectile. However, the collision causes the impact bar to be elastically compressed. Therefore, the end of the bar is displaced in the direction of the impacting projectile a distance w

$$w = \int_0^z \epsilon dz \quad \text{Eq. (e)}$$

$$= c \int_0^t \epsilon dt \quad \text{Eq. (e')}$$

where c is the velocity of sound. Thus, penetration is given by

$$x = z - w \quad \text{Eq. (f)}$$

and the velocity of the projectile relative to the end of the bar is given by

$$\dot{x} = \dot{z} - c\epsilon \quad \text{Eq. (g)}$$

Assuming the projectile to rebound with a velocity v_f , its change in momentum must equal the momentum imparted to the bar. This is the total time integral of the force (neglecting reflections), or

$$m(v_0 - v_f) = AE \int_0^\infty \epsilon dt \quad , \quad \text{Eq. (h)}$$

in which v_o and v_f are the (algebraic) velocities and can have positive or negative values depending on whether the motion is in the direction of the initial impact or its reverse, respectively.

In general the actual measurement of the pulse consists of a strain gage voltage reading as a function of time. This strain is presumably proportional to the strain averaged over the cross section. However, for reasons already discussed, strain at the gage itself may depart from the average strain. Assuming the average planar strain ϵ is simply proportional to the observed strain ϵ_g at the gage, i.e., $\epsilon = \beta\epsilon_g$, we can write for the correction factor β , using Eq. (h)

$$\beta = m(v_o - v_f) / [AE \int_0^{\infty} \epsilon_g dt] \quad \text{Eq. (i)}$$

Wherever ϵ appears in the preceding equations, this should be replaced by $\beta\epsilon_g$. Thus, in principle, the striker velocity \dot{z} , penetration velocity \dot{x} , penetration depth, resisting force, and other related quantities can be computed from the impact pulse.

Energy is distributed within the specimen and the bar in several ways. Some of the energy is localized near the site of the impact, e.g., that expended in the non-recoverable (anelastic, plastic, viscous) deformation process. There is also a local elastic energy stored in the impact region that subsequently is transferred back to the striker when it rebounds. Finally, there is both a distributed kinetic and potential energy associated with the pulse as it moves along the impact bar. This later energy can be compared as it develops with time. The elastic potential energy is given by

$$\begin{aligned} U_1 &= \int (\text{strain energy/unit volume}) \cdot d(\text{volume}) \\ &= \frac{1}{2} A E c \int_0^t \epsilon^2 dt \quad \text{Eq. (j)} \end{aligned}$$

From the principle of equipartition of energy, this also equals the kinetic energy of the pulse so that the aggregate distributed energy associated with the pulse is

$$U = AEc \int_0^t \epsilon^2 dt \quad . \quad \text{Eq. (j')}$$

This energy is trapped in the bar, and excites the bar vibrationally, ultimately ending up as heat.

The kinetic energy of the striker can be determined as a function of time. However, we have found no simple way as yet of computing the amount of recoverable energy as a function of time during the course of the collision. Incidentally, neither was there a way to do this in our prior work using the mechanical test machines. The final irreversible work performed on the specimen, of course, is simply the initial kinetic energy of the striker, less its recoil kinetic energy and the pulse energy U.

4.2 Integration Procedures

As can be seen from the preceding section, determination of the various penetration, velocity, energy, and correction quantities requires evaluation of the integrals $\int \epsilon dt$, $\iint \epsilon dt dt$, $\int \epsilon^2 dt$. Once the strain is available in digitized form, the evaluations are straightforward using standard computer techniques. The uncertainties arise primarily from the impact pulse itself. In principle, the pulse should rise from a base line, representing the zero strain condition and should then return to the same base when the striker, upon rebound, breaks contact with the target. However, this idealized situation is usually not observed. The possible reasons for this will be discussed in Section 5. As discussed in 4.1, the value of the correction term β depends on the value of the integral of strain over the duration of the total pulse. Assuming the shape of the

pulse to be correct in other respects, an incorrect assignment of β will lead to such computational aberrations as the striker continuing to exert a reaction force after it has left the specimen. Hence, a way of dealing with this situation is required. This will be considered again in more detail in 4.4 following the presentation of typical computations on the pulse information in Section 4.3.

In summary, starting with the record of the pulse from the strip chart recorder and the experimental observations, the procedure for analyzing the data can be outlined as follows:

- (1) Determine the momentum change in the striker and the momentum imparted to the impact bar. Compare. Average the values.
- (2) Convert the recorded pulse into digital form.
- (3) Translate the digital information into time and strain units.
- (4) Compute the various time integrals of strain.
- (5) Determine the calibration factor β .
- (6) Compute the kinematic information such as penetration depth, force, striker translation, striker velocity, pulse energy, bar momentum, as a function of time using the equations in 4.1.
- (7) Compute correction for the extended long-term tail on the pulse. (See 4.4.)
- (8) Repeat steps 4 to 7 using corrected pulse.
- (8) (Alternative) Fourier analyze corrected pulse.
- (9) Reconstruct pulse as it would be at site of impact.
- (10) Repeat steps 4 to 7 using reconstructed pulse.

Items 8(Alternative) and 9 are explained in Section 4.5

4.3 Momentum Measurements

Determination of the momentum change in an impact is basic to the determination of the correction factor β . Conservation of momentum requires that the change in momentum

of the ball must be exactly equal to the momentum imparted to the impact bar (or other parts of the system).

The procedure used here was to measure both the momentum change for the striker and for the bar. This was done by measuring the striker height before it was released and at the position of impact with the bar. This was done to ± 0.1 mm using a cathetometer fitted with a telescope. A correction was made for damping in the swing of the striker for a 10 cm initial swing amplitude as shown in Fig. A. The damping is logarithmic and is about 5.6% per cycle. Observations on a single cycle at the amplitudes used for the impact experiments gave a decrement of 4.0% for the velocity. Thus, in the quarter cycle of a swing that occurs during an impact test, the velocity is about 1% less than the value calculated using the simple theory.

The damping of the motion of the impact bar was found to be negligible. However, there was a noticeable correction due to frictional effects for the rider that marks the horizontal movement of the bar. The rider, which weighs 0.42 g, would just move on the wire when it was tipped about 13° from horizontal. Thus, the frictional force was about 100 dynes. Since momentum is the integral of force over time, a momentum correction of 51 g cm/sec was computable from the time for the bar to swing to its maximum amplitude, 0.52 seconds. The estimated error in reading the horizontal component of the bar movement is ± 0.2 mm. The velocity V of the bar and, thus, the momentum are calculable from geometries and the simple equations of motion using

$$V = [2g(R - \sqrt{R^2 - L^2})]^{1/2}$$

where L is the amplitude of the swing, R is the length of the bar supporting thread, and g is gravitational acceleration.

Even with these refinements, the momentum as computed from the striker data was 2.2% greater than that computed from the bar movement, the range of the absolute standard deviation being $\pm 1.2\%$. The reason for this systematic bias is not known. The greatest uncertainty in the measurements results from the error in reading the rider position. This is estimated to result in an error of $100 \text{ g cm sec}^{-1}$, which is between 1% and 2% relative error and is less than the systematic value. In making the estimates for β , the average value has been used.

4.4 Correction for Post-Pulse Behavior

Ideally an experimentally observed pulse is preceded by a steady, zero-strain signal from the strain gage. The signal should again return to this zero-strain level following the passage of the pulse, i.e., after the striker has rebounded and there is no reaction force possible. In practice a steady pre-pulse signal is usually observed, but the post-pulse level does not always return to this value.

In the case of impacts with the glass targets, the post-pulse signal often exhibits a kind of low amplitude oscillation with a period that approximates the pulse duration. After some "hunting" the value approaches the original pre-pulse level. This is shown in Fig. A for the case of a 4.5 mm diameter, 42 g striker impacting a glass target at 2.45 m per second. In contrast, when the target is a polymer, the post-pulse signal is quite steady, often slowly diminishing and persists for long times at levels appreciably different from the pre-pulse value. The extended pulse resulting from a similar impact as just described but with PC as the target is given in Fig. B.

At this time it is not certain what is causing the extended "tail" in the case of the polymer impacts. Based on our previous work, it seems reasonable that plastic flow or the somewhat delayed strain relaxation in the region of the impact are involved. Residual internal strains in the bar would seem to be

eliminated from consideration because the strains produced in the bars are relatively low $<10^{-3}$, and the post-pulse behavior depends on the target, whereas the level of strain produced is about the same in all of the impact experiments. This can be seen in Table 3.4A.

However, for purposes of carrying out the various integrations outlined in 4.2 and for getting as "clean" a base pulse for subsequent analysis, a procedure for correcting the pulse for this tail would be beneficial. A procedure for accomplishing this has been developed based on the assumption that (1) the tail is linearly extrapolatable to short times from its behavior at long times, and (2) that for times less than corresponding to the peak strain, the amplitude of the tail component increases proportionally with strain. In addition, we require that at the moment the striker breaks contact with the target upon rebound, force can no longer be exerted on the target.

Thus, a methodology has been developed which is based upon self consistency with the simple laws of nature which require conservation of momentum on the one hand and transfer of momentum only as long as the impacting bodies are in contact. For example, by requiring that the tail amplitude has a given value at some selected time, a slope is defined by this procedure. This provides a description of the tail, which can then be subtracted from the observed pulse to give a corrected pulse.

However, the use of this procedure will become more important after a satisfactory method has been achieved for correcting the pulse for changes of its shape as it travels down the bar. This is discussed in more detail in Sections 4.5 and 4.6

4.5 Studies Using Inorganic Glass Targets

Because of the uncertainty regarding the process that extends the tail of the impact curve and the absence of a priori information as to what the pulse shape should be when a polymer is impacted, the impact between a steel projectile and an inorganic glass specimen was examined in some detail. The completely elastic behavior of glass makes it possible to calculate the pulse shape from the Hertz analysis.

The computed pulse shape could then be treated as if it had been experimentally obtained and introduced into the computer programs for computing velocities, penetrations, etc. This procedure provided confirmation of the validity of our computational apparatus. Then by experimentally impacting a glass specimen, we were able to compare the pulse with the theoretically computed pulse. Furthermore, the studies with glass allowed examination of the question of the importance of acoustic impedance matching between the specimen and the impact bar. These points are covered in more detail in the sections that follow.

As an unexpected by-product, we discovered that the glass when struck by the steel striker produced a nearly dead impact, i.e., with very little rebound of the striker. In contrast, a polymer target when struck results in a substantial rebound. This observation was contrary to our intuition, and its examination led to further insight into the impact process.

We had expected the glass target to result in a greater recoil than in the case of the polymer because no significant inelastic processes would be involved. Instead the striker upon impact behaved almost as if it had struck putty. This was a general phenomenon that occurred whenever the target material mounted onto the end of the PMMA impact bar was a stiff elastic material, e.g., silicon carbide, tungsten carbide, hardened steel. Our initial hypothesis was that the acoustic impedance mismatch was somehow preventing the pulse from propagating into the bar.

However, the answer was found to be in the elastic energy expression, Eq. 4.1j', and the ce term in Eq. 4.1g. The combination of a very stiff target and a relatively compliant impact bar causes substantial compressional shortening of the bar and a large amount of energy to pass into the impact bar. As the striker reacts against the hard target material, it causes the struck end of the bar to accelerate in the direction of the impact. By the time the striker slows down, the end of the bar is moving away from it fast enough for the penetration depth to be substantially reduced at this point in time. Hence, from the Hertz relationship it is clear that the force available to push the striker back is accordingly also reduced. Thus, most of the kinetic energy initially present in the striker is now associated with the pulse that is traveling down the bar.

4.5.1 Theoretical Elastic Impact Pulse. The usual expression for a dynamic elastic impact by a ball on a planar surface is given by relating the deceleration force F to the indenter travel z through the Hertz law

$$F = kz^{3/2} \quad \text{Eq. (a)}$$

where

$$k = \frac{4}{3} \sqrt{R} \left(\frac{1 - \nu_1^2}{E_1} + \frac{1 - \nu_2^2}{E_2} \right)^{-1},$$

ν being the Poisson ratio, E the Young's modulus for the target and striker materials, and R the radius of curvature of the striker. If m is the mass of the ball then

$$-m\ddot{z} = kz^{3/2} \quad \text{Eq. (b)}$$

This equation can only be solved approximately. However, maximum incursion depths, time of contact, etc., can be found in various standard works. Note that the equations (a) and (b) are reversible. Thus, an ideal loss-less, elastic collision is predicted by this model.

However, as noted in Eqs. 4.1f and g, it is the incur-
sion depth x and not the travel z that determines the force.
That is,

$$- m\ddot{z} = k(z - c \int_0^t \epsilon dt)^{3/2} \quad \text{Eq. (c)}$$

should replace Eq. b. This somewhat awkward equation can be readily integrated by computer. The solution in terms of the force versus time and of the striker velocity versus time is given in Figs. A and B. As can be seen, the inclusion of the bar compliance results in a distinctly skewed impulse curve and predicts that the rebound velocity will be much less than the impact velocity even with ideally elastic materials. Thus, the correction for the motion of the target has a major qualitative effect. This computation was made for the example of a 19 mm steel ball impacting a glass target mounted on the end of a PMMA impact rod.

When the theoretically derived impact curve is introduced into the analytical apparatus for deducing the force penetration law responsible for the observed pulse, the Hertz law behavior is deduced. In other words, assumption of the Hertz law allows synthesis of the pulse shape. Analyzing that pulse shape reveals and confirms that the Hertz law governs the pulse. Hence, the analytical procedures and associated computer programs we have developed are valid.

4.5.2 Critical Experiments. As discussed above glass is an ideal medium for testing the impact bar equipment and for allowing straightforward comparison between theory and observation. The work described in this subsection had the dual goals of (1) establishing the validity of the procedure in which specimens are mounted onto the striking ends of bars of another material, and (2) providing a direct comparison between an observed pulse and a pulse computed from theory using the same input conditions.

In Section 3.1.1 the problem of acoustic coupling between the specimen and the bar was briefly discussed. When the target material mounted on the PMMA impact bar is glass, the ratio of the acoustic impedance of the bar to that of the specimen is 1:5. By contrast, when the target is PC or epoxy, the impedance match is typically 3:4. If the bar itself is the target or if the target and bar are made of the same material, there is no mismatch. However, in the latter case, the coupling resin could conceivably cause signal distortion.

In order to test to what extent the signal is affected by less than perfect coupling, the following experiments were performed:

(1) A 25 mm diameter Pyrex rod, 1.3 m long, has SR-4 strain gages applied to it, analogously to the PMMA impact rod. The bar was held with the long axis vertical and a 19 mm diameter hardened steel ball dropped on the instrumented end from a height of about 22 mm. This produces an impact velocity of about 1 m per second. The pulse was detected and recorded using the same instrumentation as used with the PMMA bar. Because of the greater stiffness of the glass, more amplification was needed. The resulting pulse is shown in Fig. A.

(2) The same instrumented glass bar as used in (1) above had a Pyrex glass specimen mounted on the end to be struck using the standard acoustic coupling resin. The observed pulse produced by a nominally identical impact is shown in Fig. B.

(3) The standard PMMA instrumented impact bar was held vertically, a Pyrex glass specimen attached to the end to be struck as in (2) and subjected to the same kind of impact as before. In this case less amplification gain was required. The resultant pulse is shown in Fig. C.

As can be seen, the pulses in (1) and (2) are identical within the noise uncertainty of the measurement. The pulse

in (3), requiring less gain, has considerably less relative noise content, but otherwise appears to be identical with the other two. Thus, except for possible subtleties obscured by the noise, there are no major qualitative differences attributable to the method of mounting the specimen to the acoustic match of the impact bar with the target specimen. It may be noted that there was a strong rebound of the striker in experiments (1) and (2) but a "dead" response in (3).

The second major reason for measuring the impact response of glass was to investigate the reason for the observed soft response during the very initial stages of impact. This was noted in preliminary experiments with PC and PMMA specimens. As may be recalled from our earlier work using the mechanical test machines, deciding when the first moment of contact occurs is often difficult. Based on the assumed validity of the Hertz law, plotting (force)^{2/3} versus time and extrapolating to zero force often provided an unambiguous determination of the time of first contact. The slope of this curve is related to the compliance of the material. In the case of the present experiments using the polymer targets mounted on the impact bar, a similar procedure could be followed using the initial portions of the pulse. However, the slope was anomalously low by about an order of magnitude. Therefore, the determination of the pulse shape for glass, in which the Hertz constant is unique because of its near-ideal-elastic behavior, provides a powerful tool for investigating this effect. Furthermore, it would be obviously satisfying to get good detailed agreement between the observed pulse with that calculated from theory.

The observed and the theoretical pulses corresponding to a 19 mm steel ball striking a Pyrex specimen attached to a PMMA bar with an impact velocity of 1.74 m per second is given in Fig. D. As can be seen, there is good correspondence in the general shape in the vicinity of the maximum. However, the gradual tapering ramp on the leading edge of the experimental pulse is not predicted theoretically.

Whereas the theoretical pulse is that calculated for the struck end of the bar, actually the pulse is detected about 30 cm from the site of the impact. Hence, some distortion of the pulse can be expected as it travels due to dispersion and attenuation effects. Probably the most direct way to examine this would be to analyze the pulse in terms of its various frequency components. The pulse could then be reconstructed at some other position in time and space after applying the appropriate adjustments for the phase and amplitude values for each component. Some preliminary work in this direction is discussed in the following subsection. It is possible that other factors may contribute significantly to the (presumed) alteration in pulse shape, such as reflections, different propagation modes, etc.

4.5.3 Preliminary Fourier Analysis. As is well known, within very broad limits, any finite function of some independent variable, such as time, definable over some range of that variable, can be expressed as a Fourier sine, cosine, or both series. An alternative representation, employed here, is to express the function $f(t)$ in the form

$$f(t) = \sum_{n=0}^{\infty} A(n) \sin (2\pi n v_0 t + \delta_n) \quad \text{Eq. (a)}$$

where $A(n)$ is the amplitude of the n th harmonic of the fundamental frequency v_0 , and δ_n is the phase shift for that harmonic. Thus, $A(n)$ represents the strength or relative contribution of a given frequency to the total function. If $f(t)$ represents the shape of the impact pulse, then the values of $A(n)$ and δ_n can be computed by well-known procedures.

If dispersion occurs, then each component frequency will travel at a somewhat different velocity. This means that if a signal is known at a given position along the impact bar, the signal at some more distant position can be determined by an appropriate adjustment of the phase, viz., by subtracting the quantity $2\pi n v_0 L / C(n v_0)$ from δ_n . The term L is the

distance between sensing locations, and $C(n\nu_0)$ is the sound velocity as a function of component frequency $n\nu_0$. By noting that Young's modulus $E = \rho c^2$ where ρ is density, the dependence of the sound velocity C on frequency can be determined from the 1974 report⁽³⁾, Fig. 7A. Over the range of current interest, this can be given by

$$C = 1.737(1 + .0481\text{Ln}(\nu))^{1/2} \text{ m/sec} \quad \text{Eq. (b)}$$

Preliminary Fourier analysis of a theoretically computed impact pulse has been performed by using a modification of a previously developed computer routine. The pulse was then shifted to a position 30.5 cm down the impact bar (corresponding to the position of the strain gage relative to the specimen force), using the procedure outlined in the previous paragraph, and using Eq. (a) to describe the dispersion. However, it was quickly recognized that there is considerable arbitrariness in this procedure because a Fourier representation predicts that the function repeats with a period corresponding to the fundamental frequency ν_0 . However, the pulse is a single event. That is, the strain gage senses a long period of no signal followed by the pulse, followed (ideally) by another long period of no signal. Therefore, for purposes of the Fourier analysis, the periods of no signal are part of the function to be analyzed. Therefore, the procedure was to add a null interval both preceding and following the calculated impact pulse. The results are given in Fig. A. The one curve shows the initial pulse calculated for the case of a 4.5 mm projectile having a mass of 42 g and an initial velocity of 150 cm per second, impacting a glass target mounted on a PMMA impact bar. The other two curves show the predicted shapes of the pulse detected 30.5 cm down the bar when the preceding and trailing null signals are 10 and when they are 200 microseconds each.

As can be seen, the predicted pulse shape is a sensitive function of the duration of the null portions relative to the actual pulse duration. Since, in principle, the null portions extend indefinitely, extending the null regions to infinity transforms the Fourier series analysis to a Fourier integral analysis. Another approach is to examine the behavior as the null portions are made increasingly longer. However, the number of computations increases as the square of the total length of the signal to be analyzed. Hence, even using a computer, this approach becomes awkward, and suggests that it may be necessary to use the Fourier integral approach instead.

In any case, dispersion appears to have the expected effect of extending the leading edge of the pulse as it moves down the impact bar. More work is needed to establish whether this accounts for the departures of the experimentally observed pulses from the theoretical computed ones, as shown in Fig. 4.5.2D.

4.6 Treatment of Pulse Data

4.6.1 Detailed Kinematic Analysis. Sections 4.1 and 4.2 discussed the basic equations needed to convert the pulse curves into information regarding reaction force, penetration depths and velocities, ball velocity, various energy and momentum terms, etc. The observed pulse results from an impact between a steel striker and a glass target fixed to a PMMA bar have been analyzed as have the experimental pulse data for two cases when the target was PMMA. In addition, theoretical pulses for the steel glass encounter were computed under identical impact conditions as were experienced in the experiments. The remaining data have not been processed as yet because it appears at this time that some kind of a pulse shape correction, such as discussed in Section 4.5.3, will need to be applied in order

to get correspondence between the pulse shape and a valid kinematic analysis. This will be discussed in more detail later.

Table 3.4A presented the average results for several replicate measurements. However, the analyses require as input the results of particular runs. The designation for a 4.5 mm diameter, 42 g, and for a 19 mm diameter, 28.3 g steel striker impacting glass at 2.45 and 1.74 m per second, respectively, are GL3N-2 and GL1N-1. The resulting pulses have been analyzed and compared with the results derived from the theoretically expected in Table 4.6A. Specimen computer analyses for the case of the GL1N-1 impacts are given in Figs. A and B and the deduced force versus penetration relationships is shown in Fig. C for the same examples.

The analysis of the theoretical pulse reproduces, within certain errors due to numerical integration procedures, the Hertz force law assumed in the first place. However, as can be seen in Fig. C, the force law deduced from the experimentally observed pulse is quite different. As already mentioned, the apparent compliance in the experimental case is initially much greater than expected. This is believed to be caused by a distortion of the pulse due to attenuation and/or dispersion effects. Analysis on the distorted pulse leads to a fictitious force law.

Nevertheless, in many other respects, there is good agreement between the theoretical and experimental results. Striker recoil velocities are close to predicted values; hence the momenta are also in good agreement. The predicted peak force is about 20% greater than the observed value. However, it appears earlier with respect to the first detectable departure from a zero signal. Although the observed pulse width is about the expected value, the observed pulse tail stretches out to much longer times. The theoretical analysis shows that the local stored energy in the target

is completely expended in causing the striker to rebound. In contrast, the analysis of the experimental data indicates that about 10% of the initial kinetic energy of the striker remains in the impact bar after the rebound has occurred, in some form other than being associated with the traveling impact pulse.

These deviations between the experimental results and theoretical expectations, under conditions in which nearly ideal impacts are experimentally expected, was interpreted as indicating that the full analysis of the pulse data is premature at this time. Nevertheless, analysis of representative polymer data has been performed on runs PM3N-2 and PM1N-3 in which a 4.5 mm diameter, 42 g, and 19 mm, 28.3 g steel strikers having initial velocities of 2.48 and 2.56 m per second, respectively, were used to produce the impacts. These results are also given in Table A.

As can be seen the recoil velocity in the case of PMMA is appreciably greater and reflects itself in the greater momentum transfer. The peak force is substantially less and the pulse width correspondingly greater than is the case for the glass impact. This is expected from the greater elastic modulus for glass. It is interesting to note in the case of the polymer that the peak force develops earlier than the maximum penetration. This may simply be a computational artifact, or it may reflect the relaxational processes expected to occur in PMMA. Finally, the residual localized energy in the case of the 4.5 mm striker is nearly twice that calculated for any of the other experimental pulses and probably reflects a real non-reversible energy absorption.

4.6.2 Macro Kinematic Analysis. Because the fine structure of the pulse causes certain complications in the detailed analysis of force, depth, energy, etc., versus time, it is of interest to examine what kind of information can be obtained from less detailed descriptions of the pulse data. Such information was presented in Table 3.4A for the three polymers

TABLE 4.6.1 A
Kinematic Analysis of Pulses for Glass and PMMA

TARGET	GLASS		PMMA	
	Obs.	Theory	Obs.	Obs.
Striker Diameter, mm	4.5	19	4.5	19
Striker Mass, g	42.0	28.3	42.0	28.3
Impact Velocity, cm/sec	245	174	248	25.6
Experiment No.				
			<u>PM3N-2</u>	<u>PM1N-3</u>
Recoil Velocity, cm/sec	23.9	17.6	72.0	80.7
Momentum Transfer g cm/sec	11294	5422	13440	9529
Peak Force, Kg	142	100	74	88
Time to Peak Force	43	31	144	84
Time to Max. Penetration	43	31	147	88
Pulse Width at Half Peak	78	53	182	102
Pulse Duration	183	124	>413	~320
Residual Non-Pulse Energy Initial K.E. of Striker	~10 ⁻³	~10 ⁻³	.22	.07

Note: Time units are μ sec.

investigated and glass. For example, if an approximate measure of the final value of the integrals $\int \epsilon dt$ and $\int \epsilon^2 dt$ could be established, then it may be possible to estimate the non-recoverable energy that remains localized in the region of the impact.

For this purpose we note that E_1 the energy extracted from the striker, i.e., its initial kinetic energy less its rebound energy is given by

$$E_1 = p(V_0 - \frac{p}{2m}) \quad \text{Eq. (a)}$$

where p is the measured change in momentum resulting from the impact, V_0 is the velocity at impact of the striker and m is its mass. Defining $Q = t_{0.5} \cdot \epsilon_{\max}$ and $J = t_{0.5} \cdot \epsilon_{\max}^2$, we also consider the possibility that

$$k_q Q \approx \int_0^{\infty} \epsilon dt \quad \text{Eq. (b)}$$

and

$$k_j J \approx \int_0^{\infty} \epsilon^2 dt \quad \text{Eq. (c)}$$

where ϵ_{\max} is the measured peak pulse strain, $t_{0.5}$ is the time breadth of the pulse at half the peak strain, and k_q and k_j are proportionality constants to be determined. As given in Eq. 4.1h

$$p = AE \int_0^{\infty} \epsilon dt \quad ,$$

and introducing this into Eq. (b) gives:

$$k_q = p/AEQ$$

Similarly from Eq. 4.1j'

$$U_f = U(\infty) = AEC \int_0^{\infty} \epsilon^2 dt$$

which when combined with Eq. (c) gives

$$k_j = U_f/AECJ$$

The value of U_f is not known without resorting to a detailed pulse analysis. However, in the case of glass, it can be assumed that there is no non-recoverable energy left in the glass following the impact. Hence, specifically for glass

$$U_f = E_1 \quad \text{or}$$

$$k_j = E_1/AECJ$$

This cannot be assumed a priori for the other materials. Therefore, the impacts with glass will be assumed to provide a means of calibration.

The experimental results from Section 3.4 are analyzed in terms of the above discussion in the following table. The values for the bar modulus E , the sound velocity C , and the cross-sectional area A are 5.18×10^{10} dynes/cm², 2.095×10^3 m/sec, and 3.61 cm², respectively, were used when needed to compute the parameters given in the table.

The results shown in the table for k_q and k_j suggest that this macro approach can give interpretable quantitative information, and the constancy of k_q indicates that the impact pulses more or less scale in a regular way. The major departure occurs in the case of the impact on glass at low velocity. The two impacts on glass give values for k_j that differ by merely 5% for rather disparate impact conditions. Taking the average value 0.74 allows computation of the ratio of the energy estimated to be tied up with the traveling pulse relative to the energy transferred to the target and impact bar, i.e. $(k_j AECJ)/E_1$. These results suggest that the impacts using the 19 mm striker are substantially reversible, if not elastic. However, with the 4.5 mm striker, the amount of irreversible work increases in the order $G < PM < E_p < PC$. This seems to be in accord with expectation.

TABLE 4.6.2 A

Analysis of Impact Using General Pulse Shape Parameters

Striker Diameter, mm	4.5				19			
Striker mass, g	42.0				28.3			
Target	PC	Ep	PM	G	PC	Ep	PM	G
V_0 cm/sec	251	250	248	245	256	260	258	174
$\epsilon_{max} \times 10^4$	3.5	3.9	4.5	6.9	4.4	4.8	5.5	5.2
$t_{0.5}$	243	217	178	93	141	124	102	53
p Kg cm/sec	14.3	14.1	13.4	11.3	10.4	10.0	9.5	5
$Q \times 10^{10}$ sec	851	846	801	642	620	595	561	276
k_q	.90	.89	.89	.94	.90	.90	.91	1.03
$E_1 \times 10^{-1}$, Joules	1.157	1.157	1.185	1.248	.750	.828	.859	.425
$J \times 10^{12}$ sec	29.8	33.0	36.0	44.3	27.3	28.6	30.9	14.3
k_j	--	--	--	.719	--	--	--	.756
$k_j AECJ/E_1$.75	.83	.88	1.03	1.06	1.00	1.04	0.98
* Irreversible Energy	25	17	12	(-3)	(-6)	0	(-4)	2

5. DISCUSSION

The data and analyses presented in Sections 3.4, 4.5, and elsewhere demonstrate that high quality, reproducible impact pulses can be produced and that the computational tools developed for analyzing the pulses work properly. Summarizing briefly, impact measurements have been made on PC, PMMA, epoxy, and glass. The measurements on the polymers show that for a given intensity impact the compliance and amount of irreversible deformation increase in the order glass<PMMA<epoxy<PC. These conclusions are based on the macro-scale analysis of the pulse data and are in accordance with our general expectations. However, the detailed analyses of the force as a function of penetration, and penetration as a function of time are at variance with the results of our prior work and also with the predictions based on a theoretical modeling of purely elastic collisions.

The use of glass as a target material has been particularly useful in defining the nature of the problem related to the detailed analysis. Measurements on this material provide a reference base for establishing the correspondence attainable between the calculated results and actual material behavior. It is almost certain that a basis can be found by which the observed pulse can be corrected for the attenuation and dispersion effects, even though the correction formulae are not now firmly known. However, other factors must also be considered, such as contributions from surface elastic waves, shear waves, and anelastic/plastic effects.

It has already been noted and as shown by comparing Fig. 3.4I with 3.4H, the pulse becomes more complex at higher impact velocities. Increasing the impact velocity increases the content of the higher frequency components. This may require consideration of the dimensions of the impact bar's small dimension relative to the wave length of a given acoustic component. If λ is large relative to the minor dimension of the bar, then the use of Young's modulus to

define velocity is valid. If λ is relatively small, then the bar acts as a bulk solid and the bulk modulus is needed. For the case of PMMA, the sound velocity corresponding to transmission in bulk material is some 40% greater than for transmission down a long, thin bar. Thus, bar geometry can affect the dispersion corrections.

These kinds of considerations will need to be addressed in seeking to describe fully the impact process at increasingly higher velocity. The degree of refinement practically attainable will be a function of the ease of its achievement and need, and will be determined largely by experience. However, it is gratifying to note that even without a detailed analysis, much qualitatively useful information can be derived from observations of the general pulse characteristics as was discussed in Section 4.6.2.

6. ACKNOWLEDGMENT

The principal investigator acknowledges the substantial contributions of his collaborators and colleagues. The development and installation of the experimental apparatus and instrumentation and the experimental measurements were largely the accomplishments of G.F. Selden, who also developed various software and computer techniques and then used these and other programs in processing the data. Valuable consultation, guidance and assistance were provided by W.P. Minnear, especially during the troubleshooting phases of the work. Counsel and help with the electronic instrumentation from R.L. Mehan and from D.B. Sorensen and L.H. String are gratefully acknowledged.

7. REFERENCES

1. W.B. Hillig, "Impact Studies of Polymeric Matrices," General Electric CRD Report SRD-73-091, prepared under Contract N00019-72-C-0218 for Naval Air Systems Command, Dept. of the Navy, March 1973.
2. W.B. Hillig, "Impact Response Characteristics of Polymeric Matrices," General Electric CRD Report SRD-74-087, prepared under Contract N00019-73-C-0282 for Naval Air Systems Command, Dept. of the Navy, September 1974.
3. W.B. Hillig, "Impact Response Characteristics of Polymeric Matrices," General Electric CRD Report SRD-75-083, prepared under Contract N00019-74-C-0147 for Naval Air Systems Command, Dept. of the Navy, August 1975.
4. W.B. Hillig, "Impact Response Characteristics of Polymeric Materials," General Electric CRD Report SRD-76-112, prepared under Contract N00019-75-C-0320 for Naval Air Systems Command, Dept. of the Navy, September 1976.

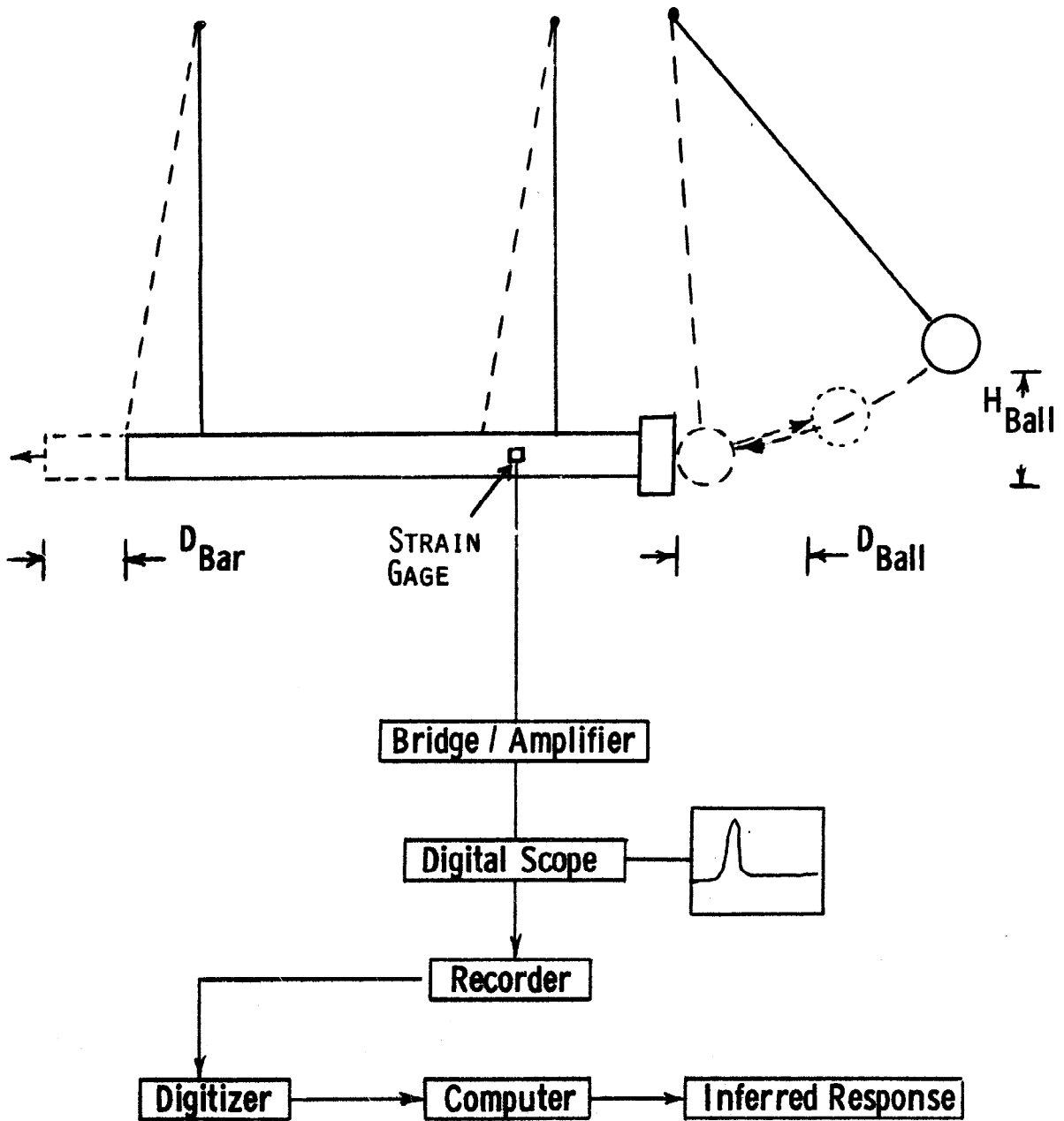


Fig. 3.1A. Impact apparatus.

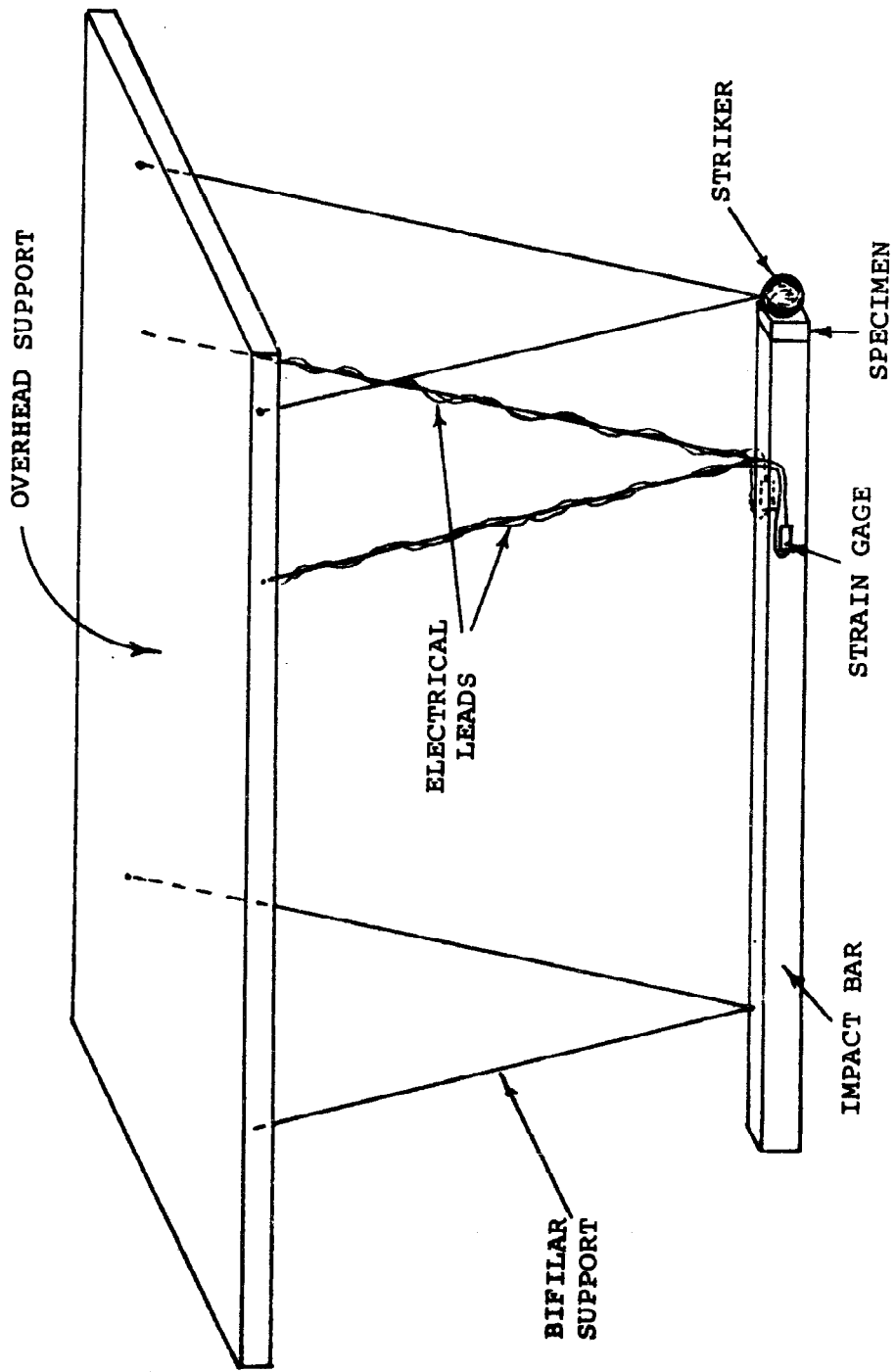


Fig. 3.1.1A. Support arrangement of impact apparatus.

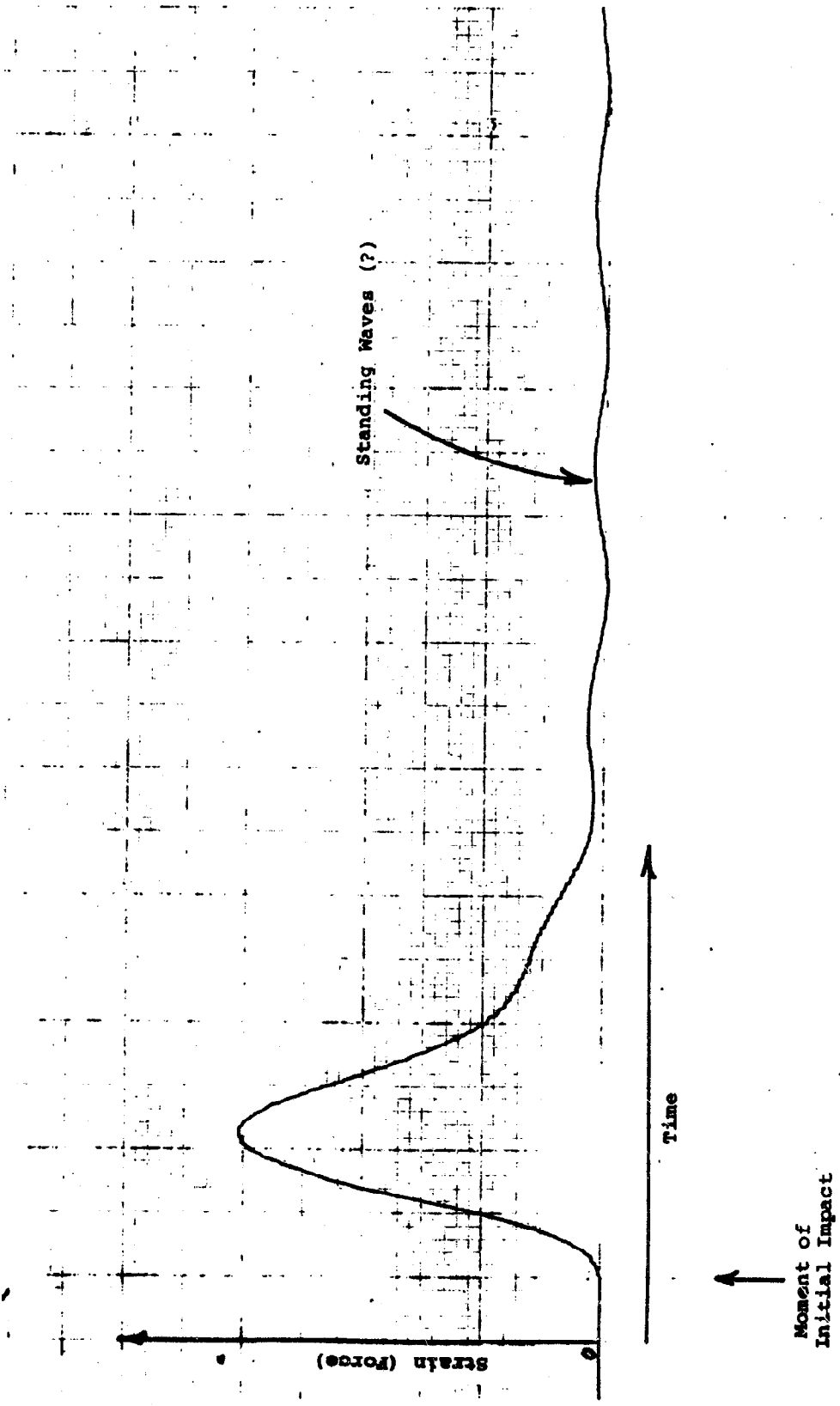


Fig. 3.1.1B. Output signal with two strain gages not located at node position.

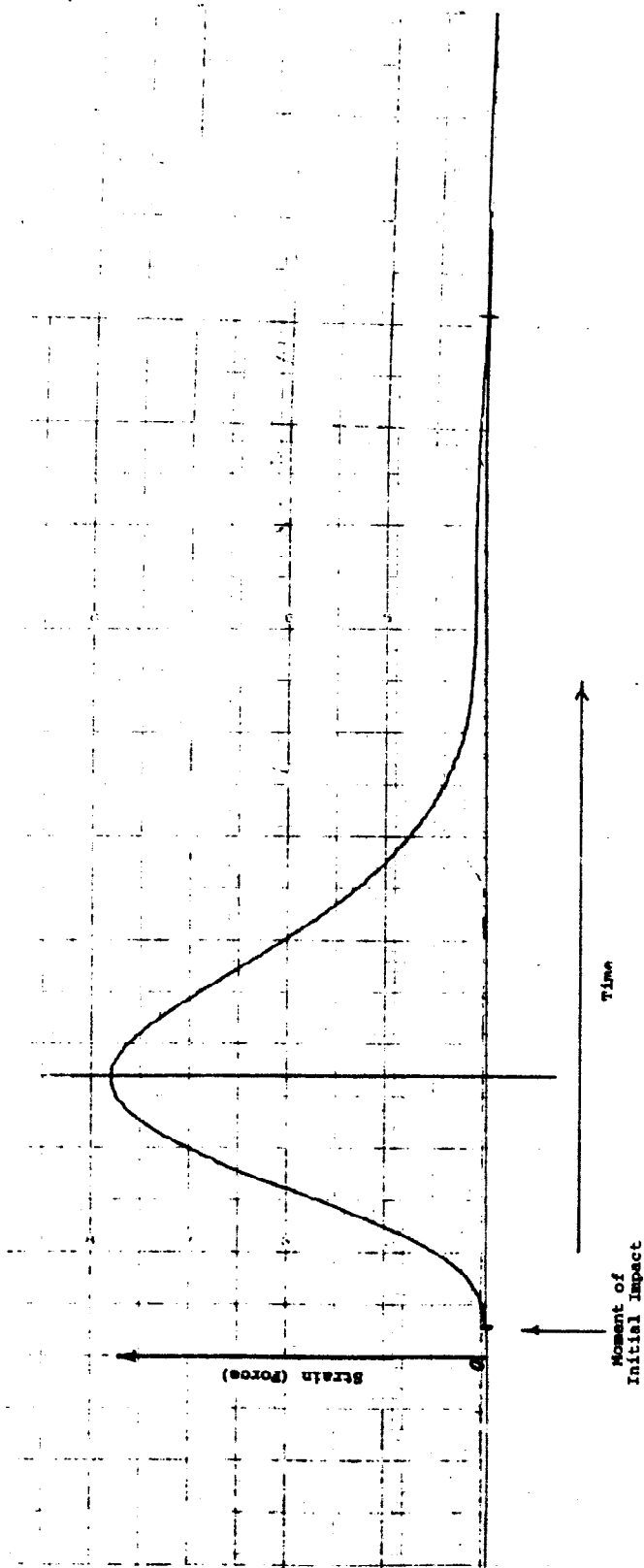


Fig. 3.1.1C. Output signal with two strain gages located at nodal positions.

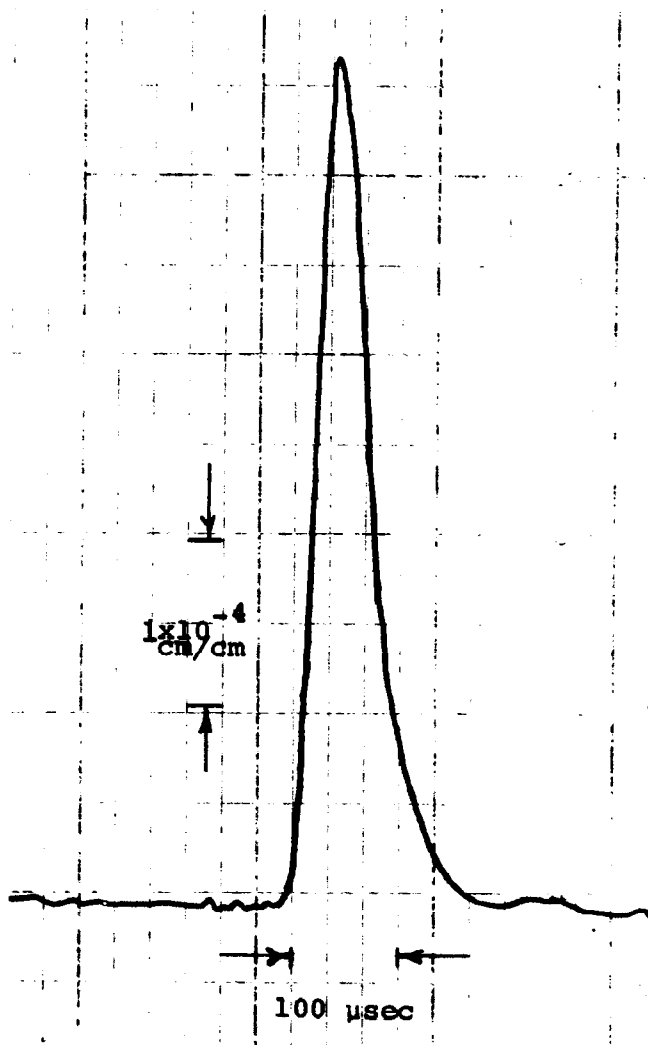


Fig. 3.4A. Strain pulse produced by impact of 19 mm diameter striker with glass target at a velocity of 174 cm/sec.

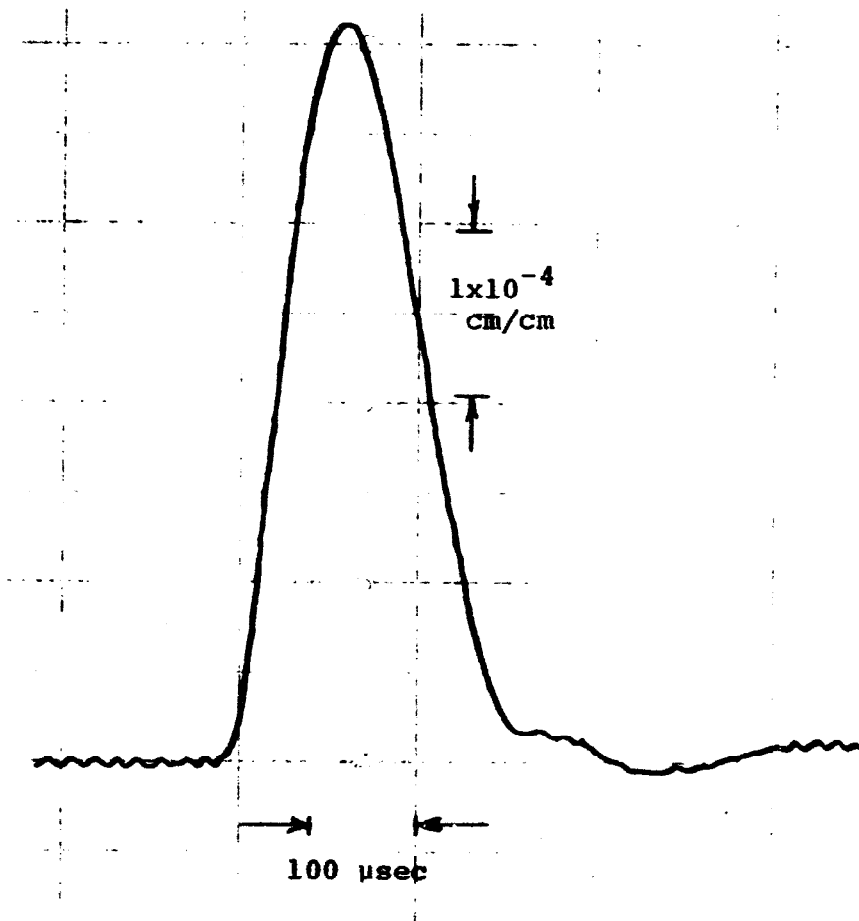


Fig. 3.4B. Strain pulse produced by impact of 19 mm diameter striker with PC target at a velocity of 256 cm/sec.

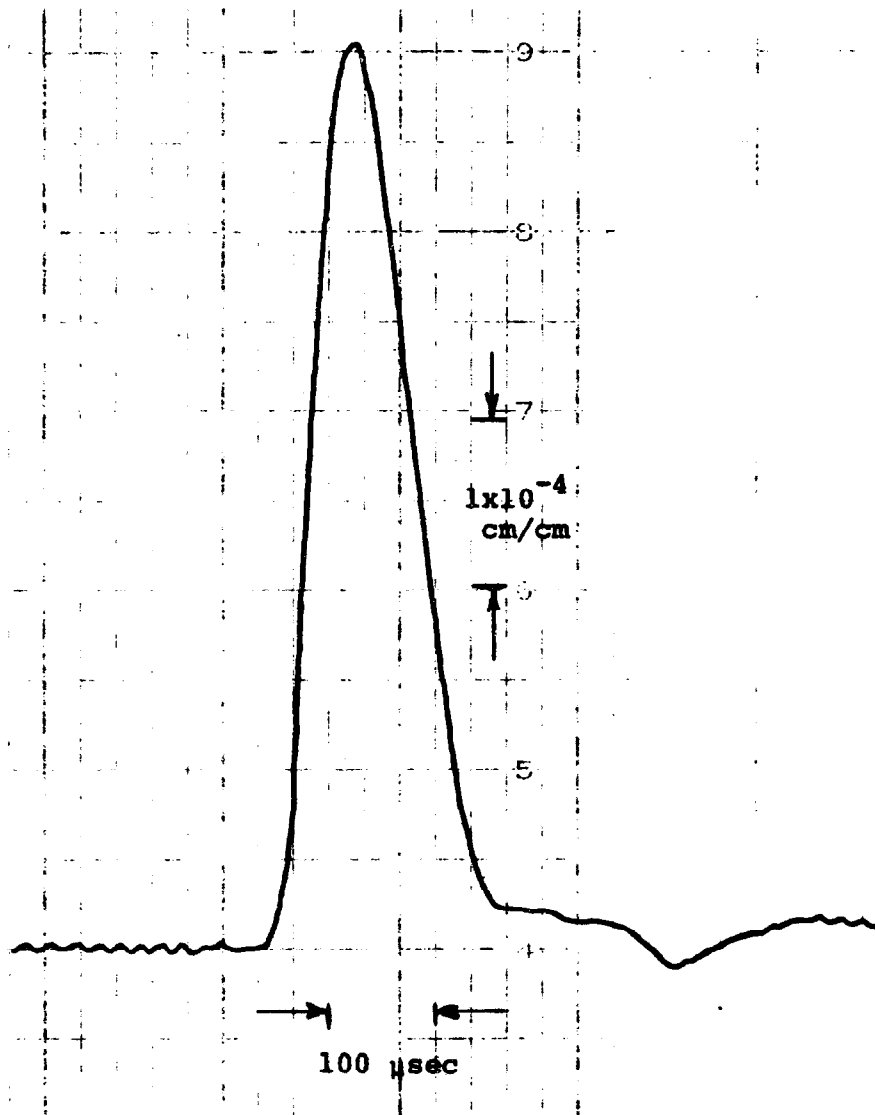


Fig. 3.4C. Strain pulse produced by impact of 19 mm diameter striker with PMMA target at a velocity of 258 cm/sec.

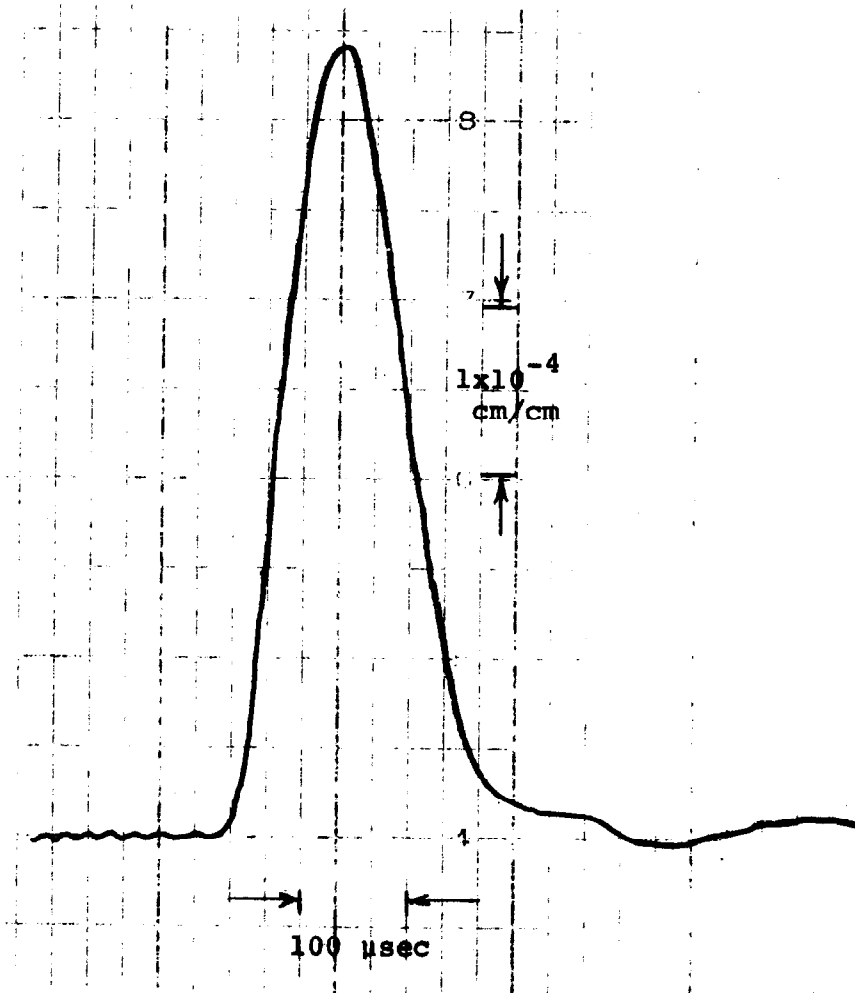


Fig. 3.4D. Strain pulse produced by impact of 19 mm diameter striker with epoxy target at a velocity of 260 cm/sec.

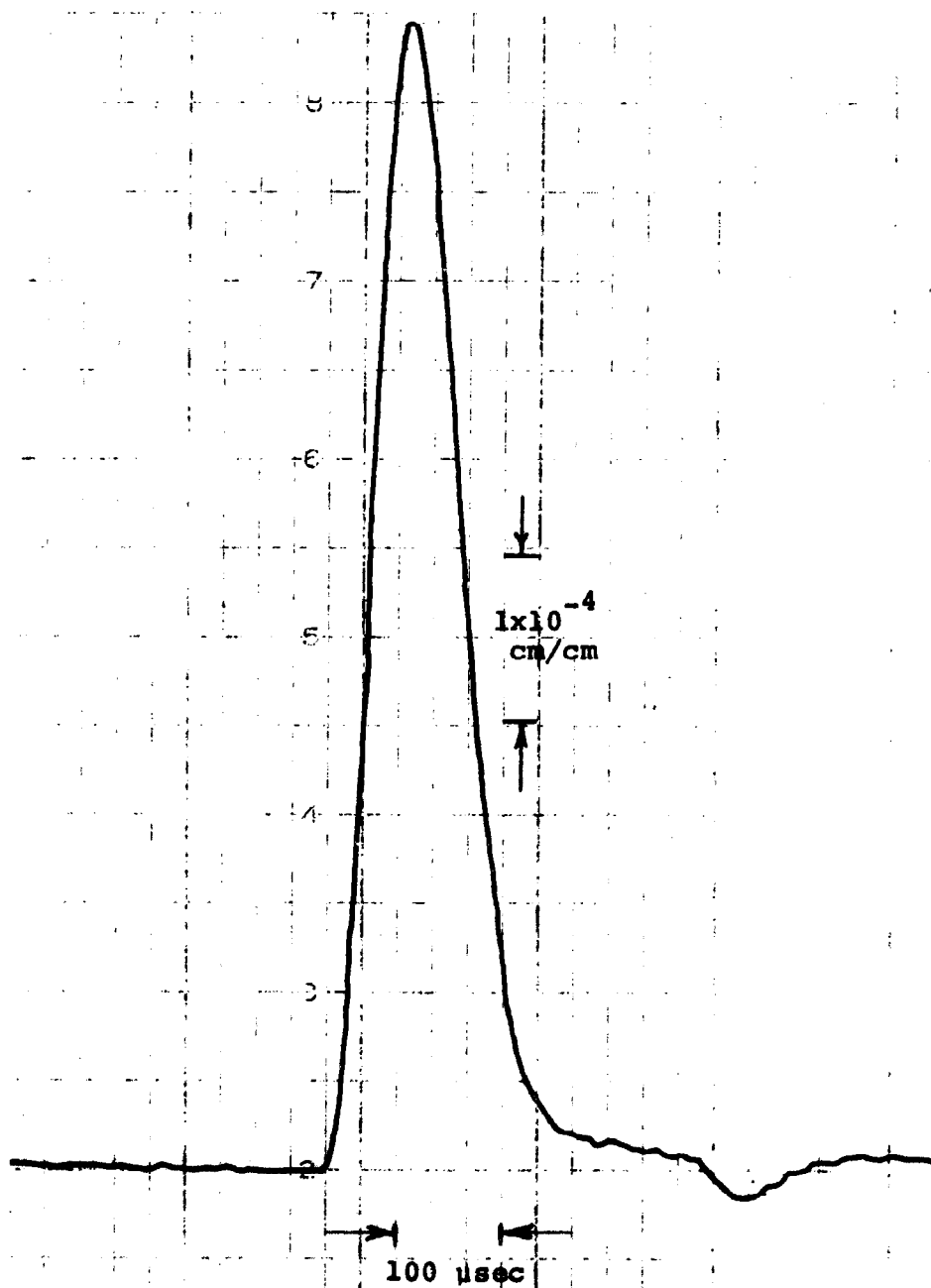


Fig. 3.4E. Strain pulse produced by impact of 4.5 mm diameter striker with glass target at a velocity of 245 cm/sec.

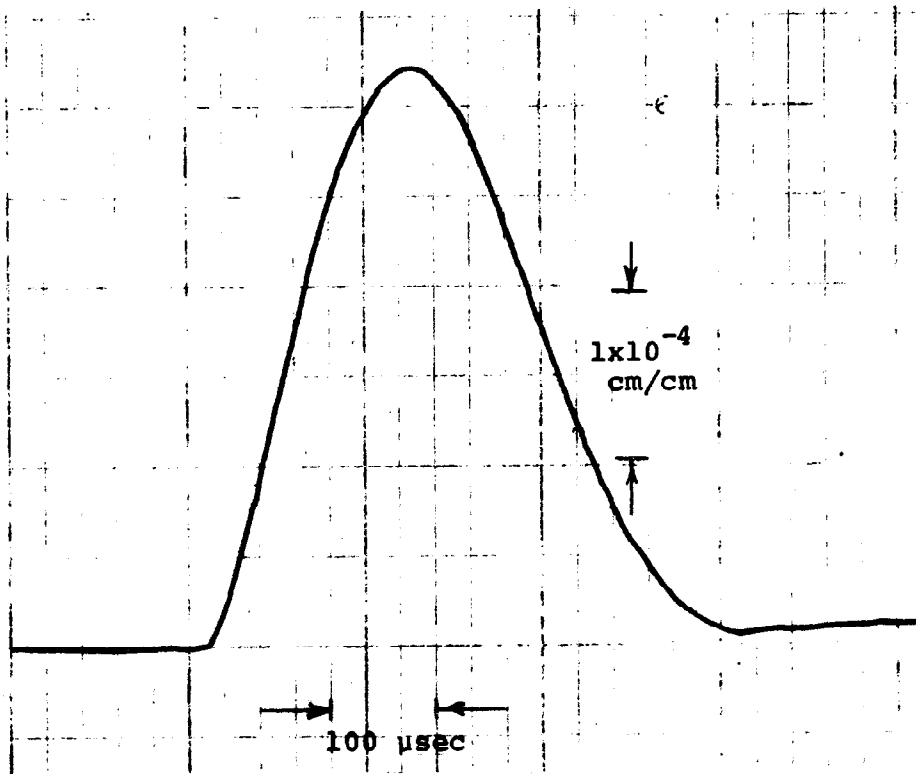


Fig. 3.4F. Strain pulse produced by impact of 4.5 mm diameter striker with PC target at a velocity of 251 cm/sec.

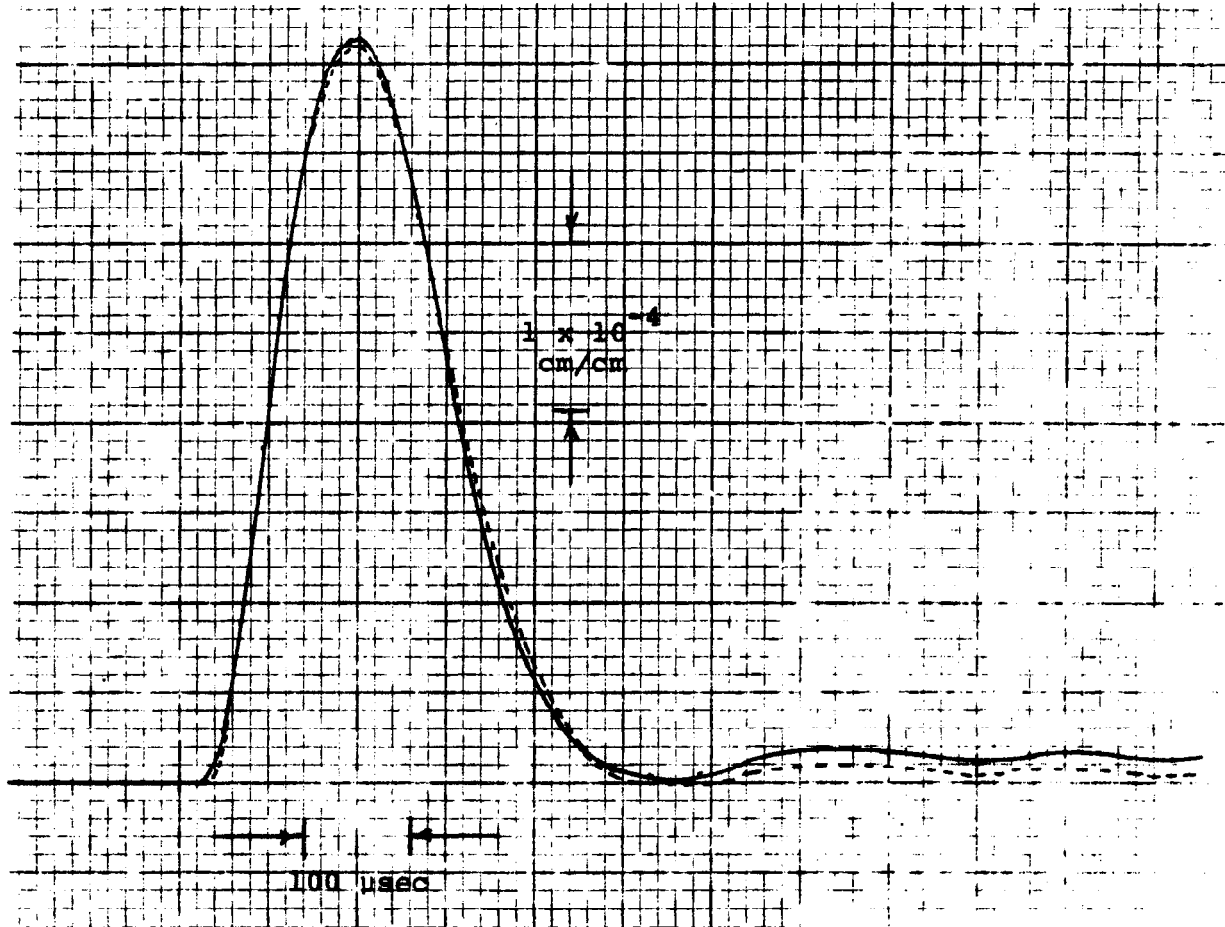


Fig. 3.4G. Strain pulse produced by impact of 4.5 mm diameter striker with PMMA target at a velocity of 248 cm/sec. Solid curve is PM3N-1; the dashed curve is PM3N-2.

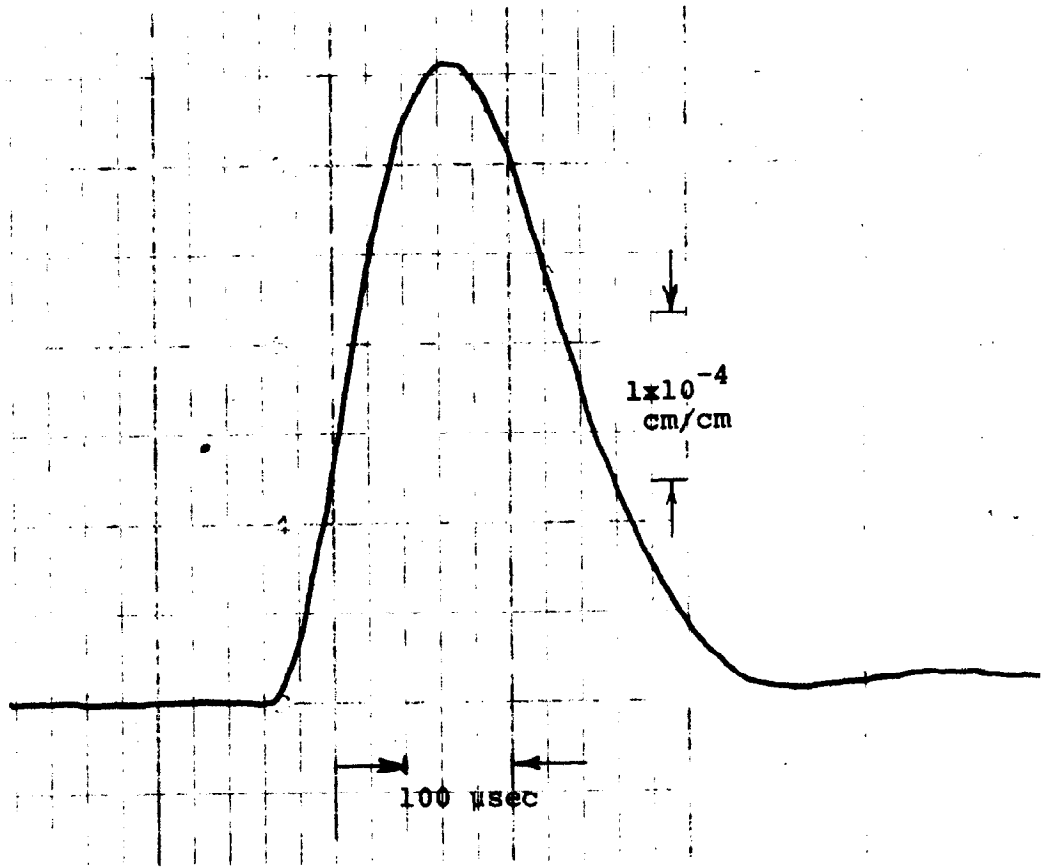


Fig. 3.4H. Strain pulse produced by impact of 4.5 mm diameter striker with epoxy target at a velocity of 250 cm/sec.

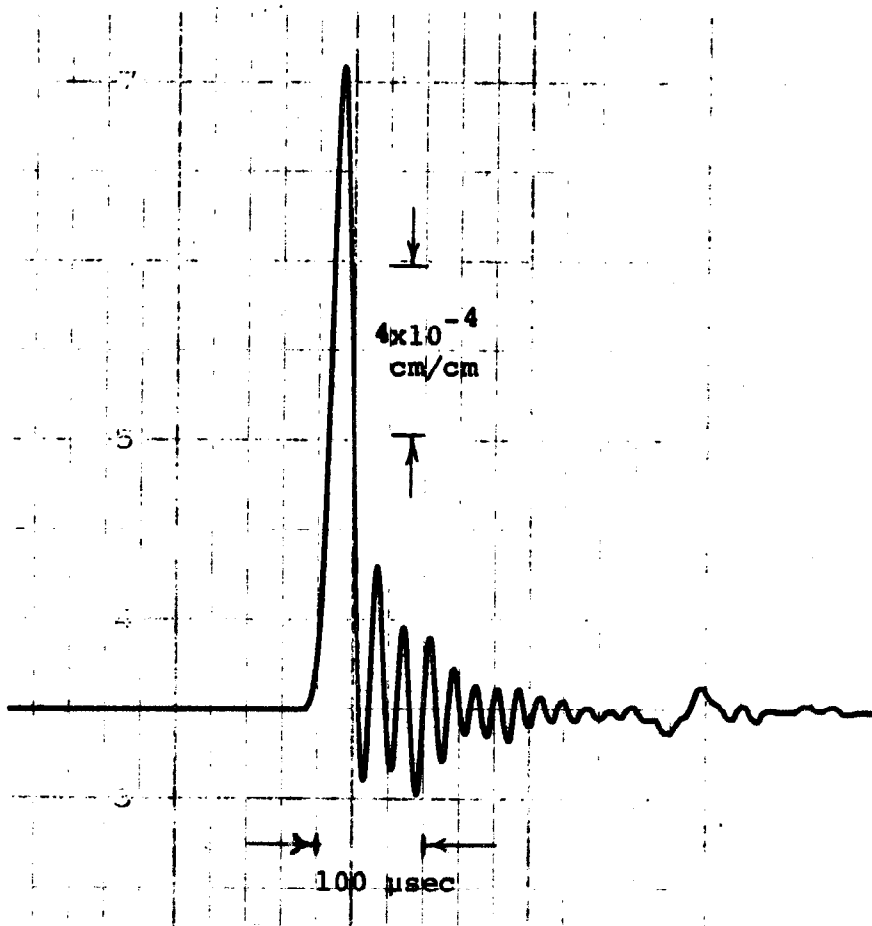


Fig. 3.4I. Strain pulse produced by impact of 4.5 mm diameter striker with PMMA target at a velocity of 100 m/sec.

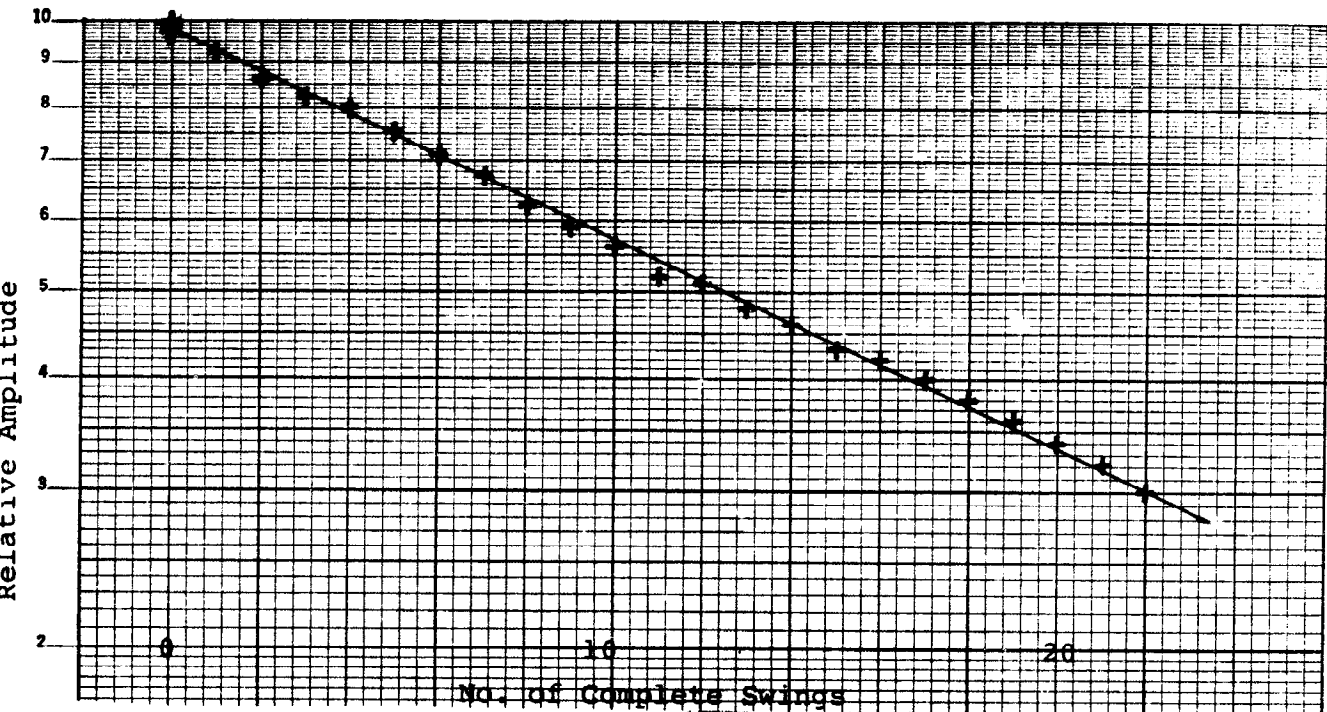


Fig. 4.3A. Damping behavior of striker.

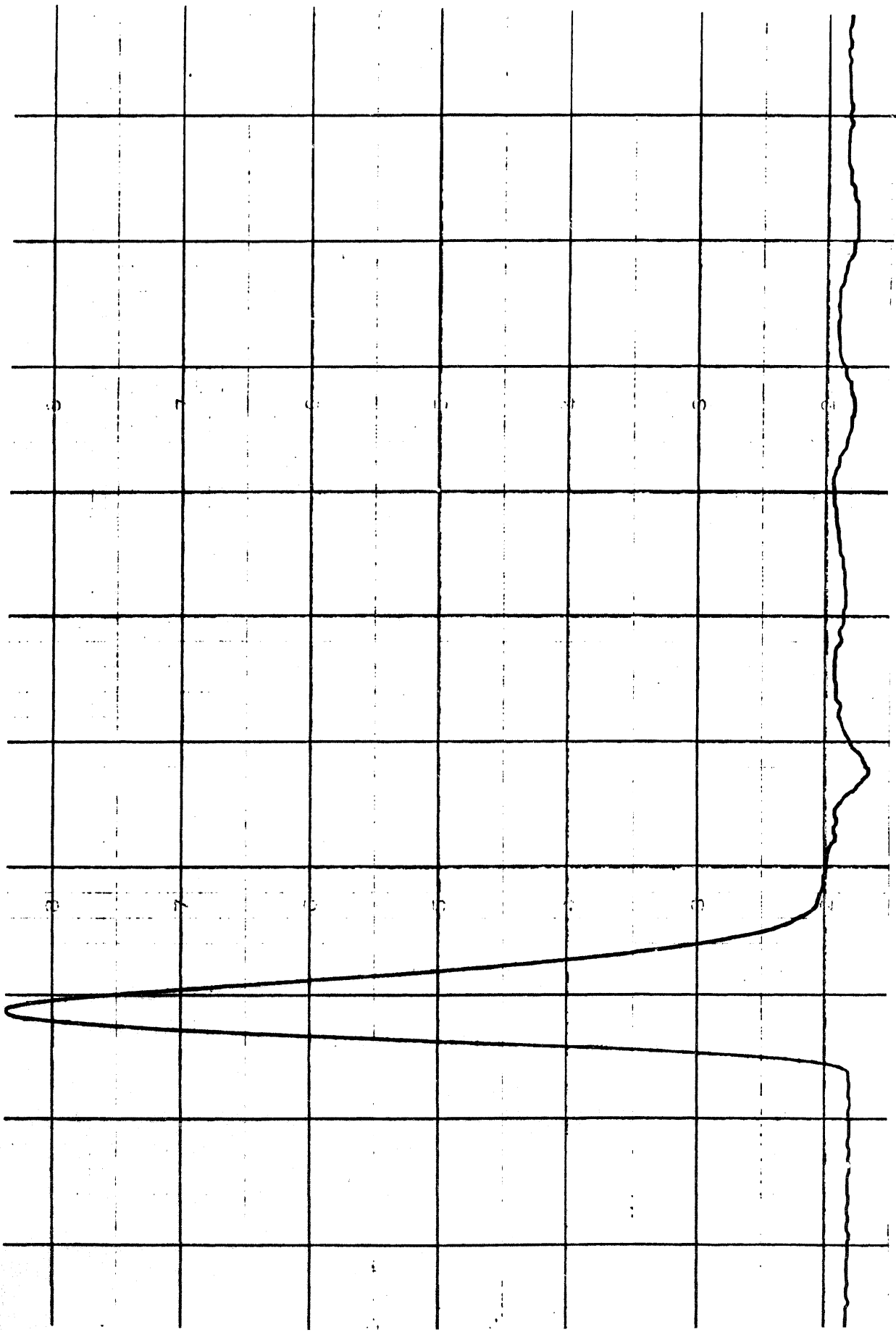


Fig. 4.4A. A typical pulse obtained using a glass target showing long-term post-pulse signal.

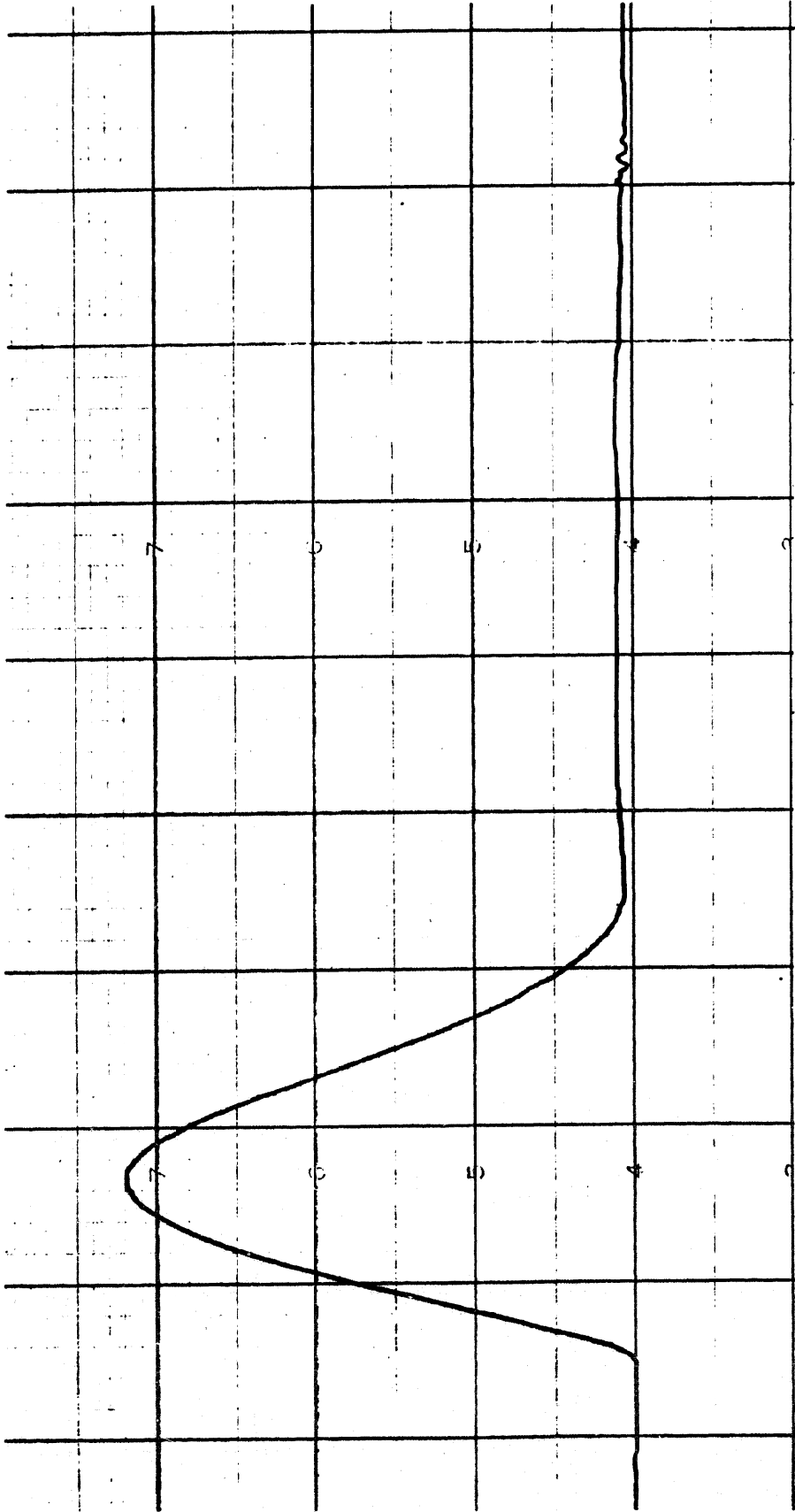
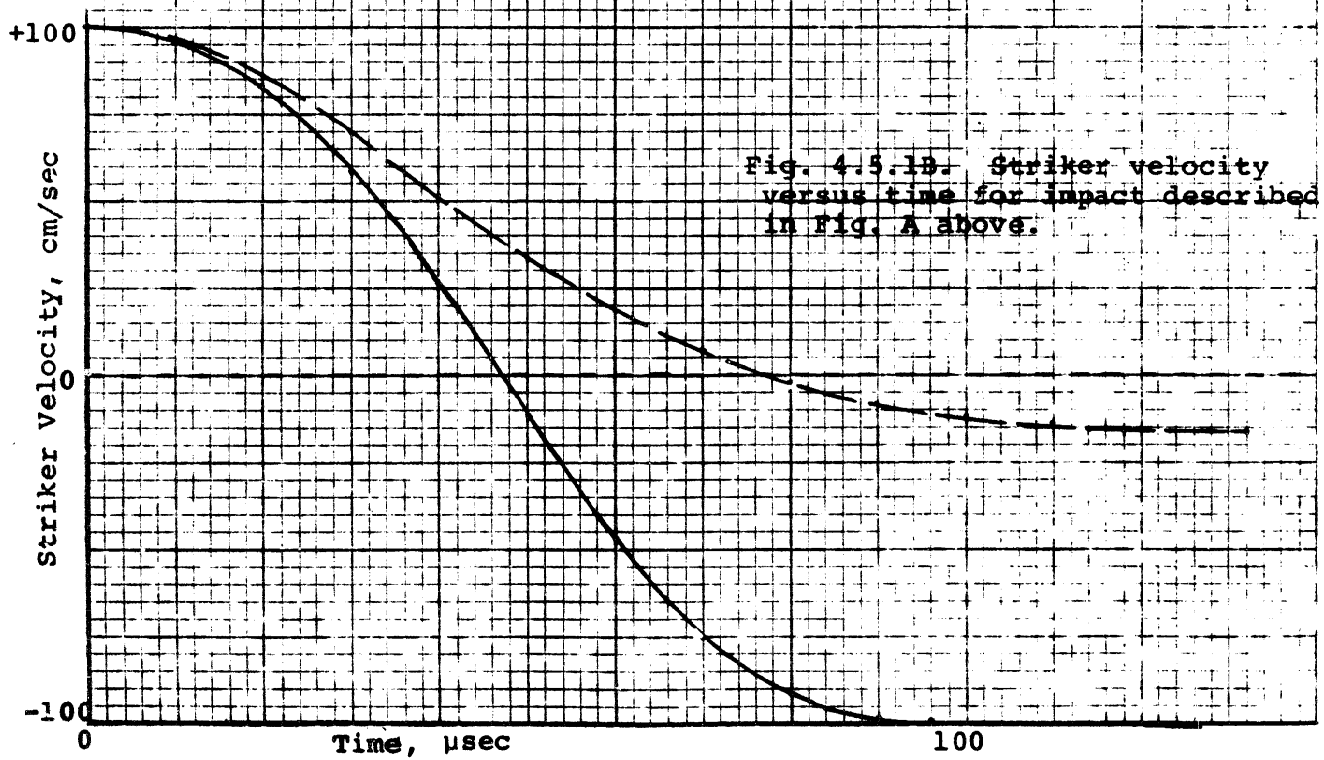
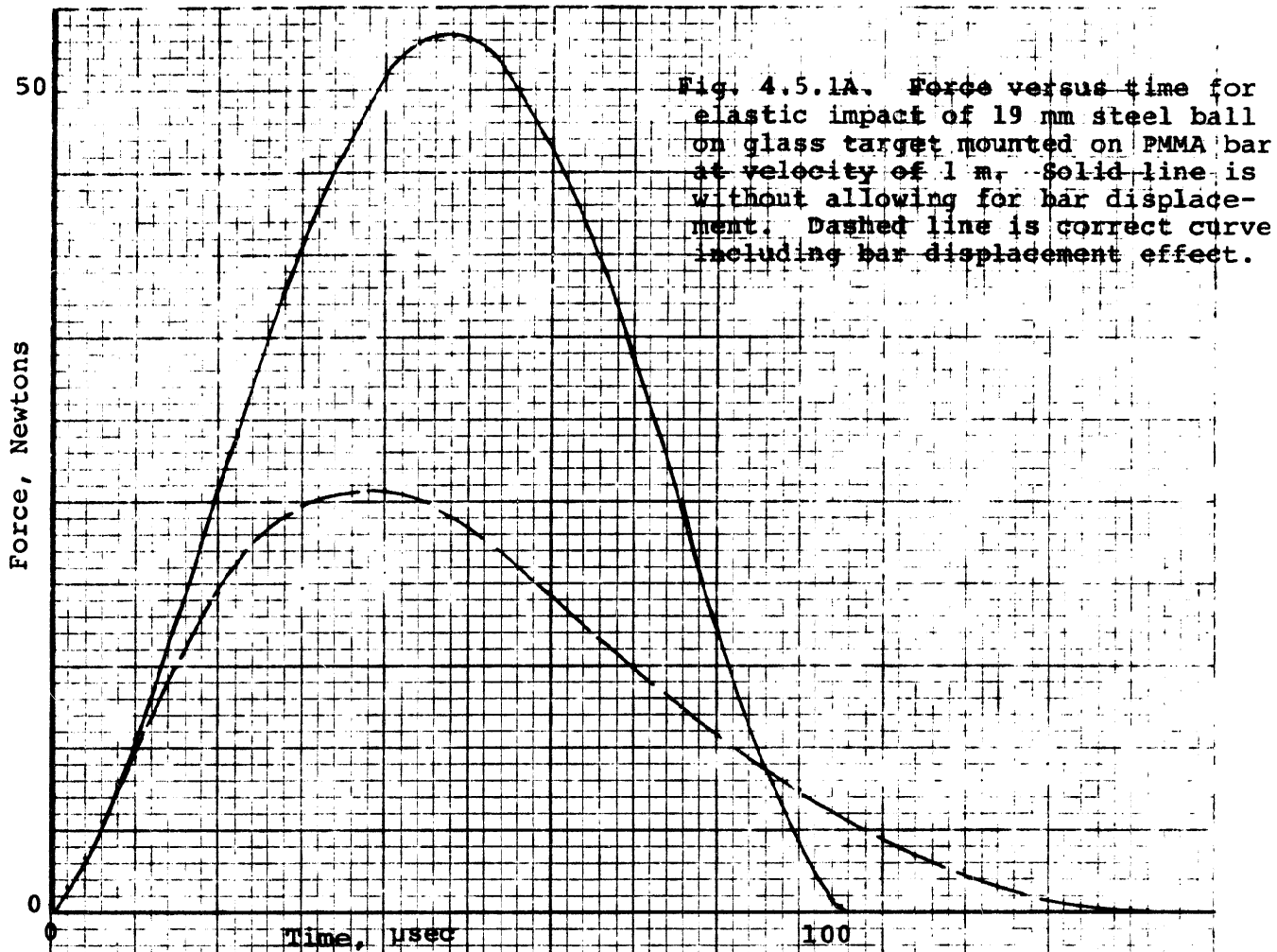
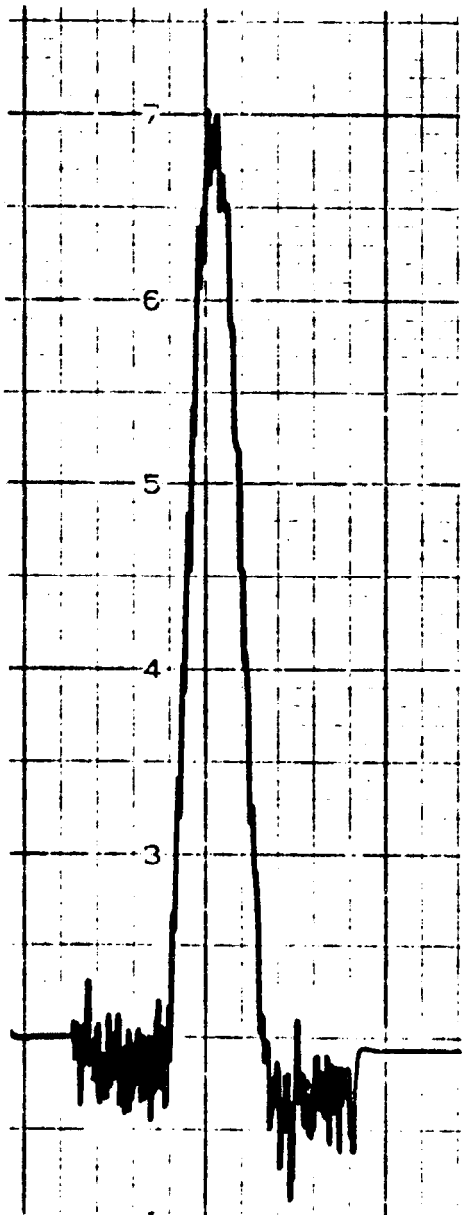
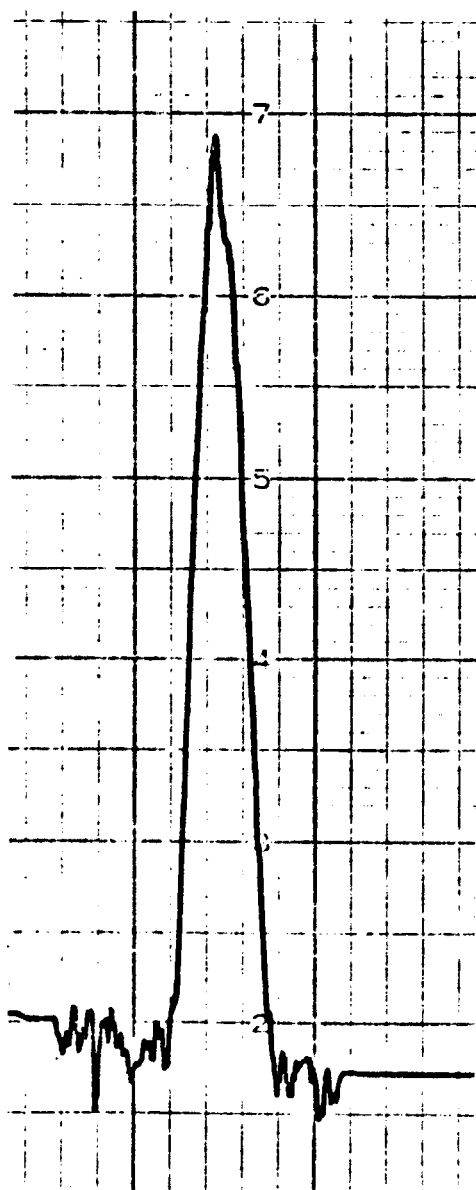


Fig. 4.4B. A typical pulse obtained using a PC target showing long-term post-pulse signal.



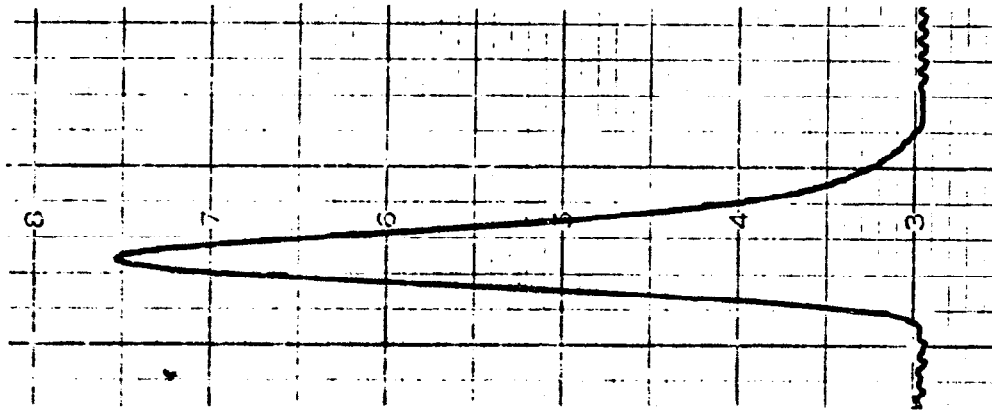


28 g Steel Ball / Glass Bar / 100 cm/sec



28 g Steel Ball / Glass Specimen / Glass Bar / 100 cm/sec

Fig. 4.5.2B



28 g Steel Ball / Glass Specimen / PMMA Bar / 100 cm/sec

Fig. 4.5.2C

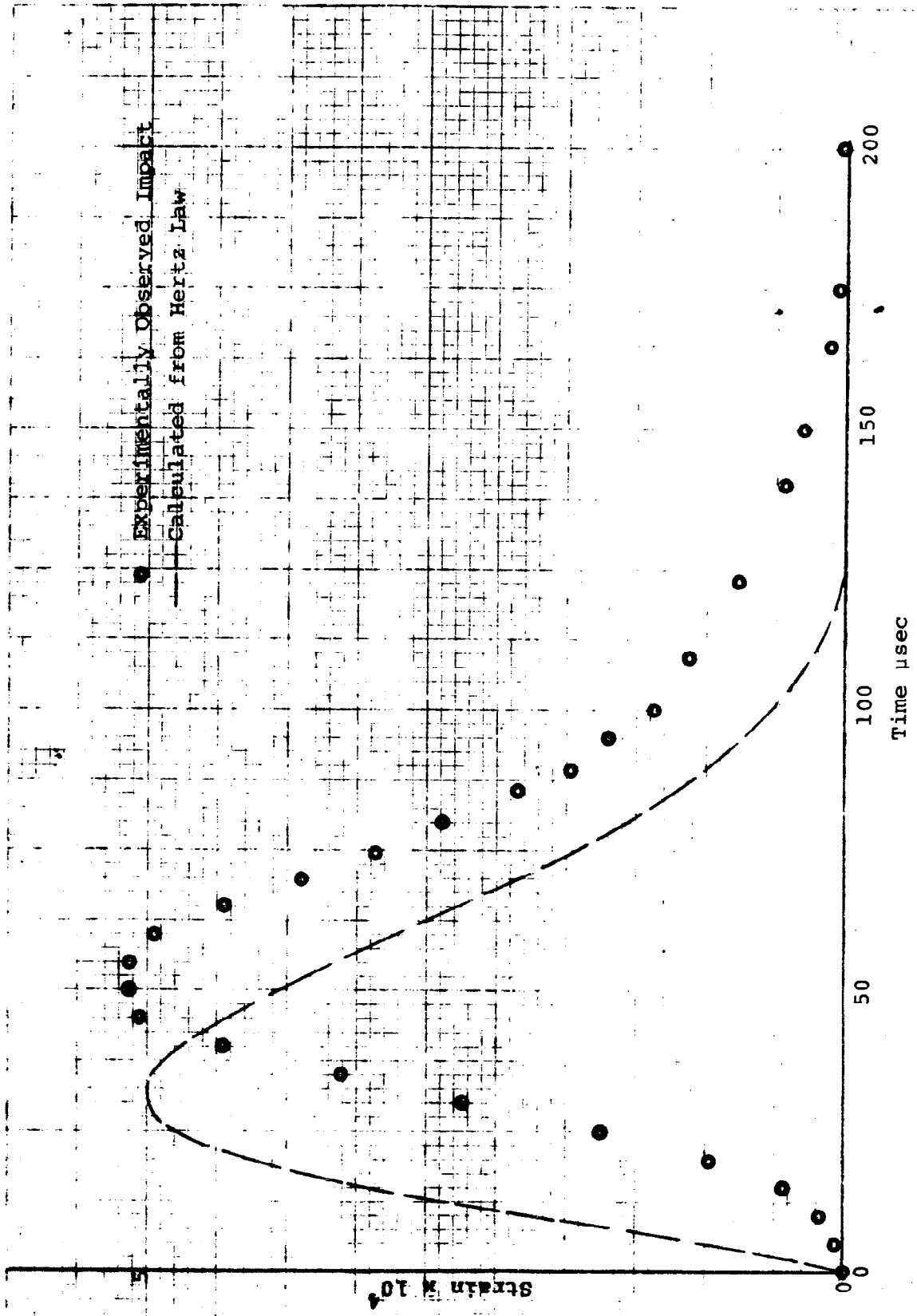


Fig. 4.5.2D. Impact pulse due to a 19 mm steel ball striking a Pyrex target on a PMMA bar.

Initial Theoretical Pulse
Shifted (10 + 10) pulse
Shifted (200 + 200) pulse

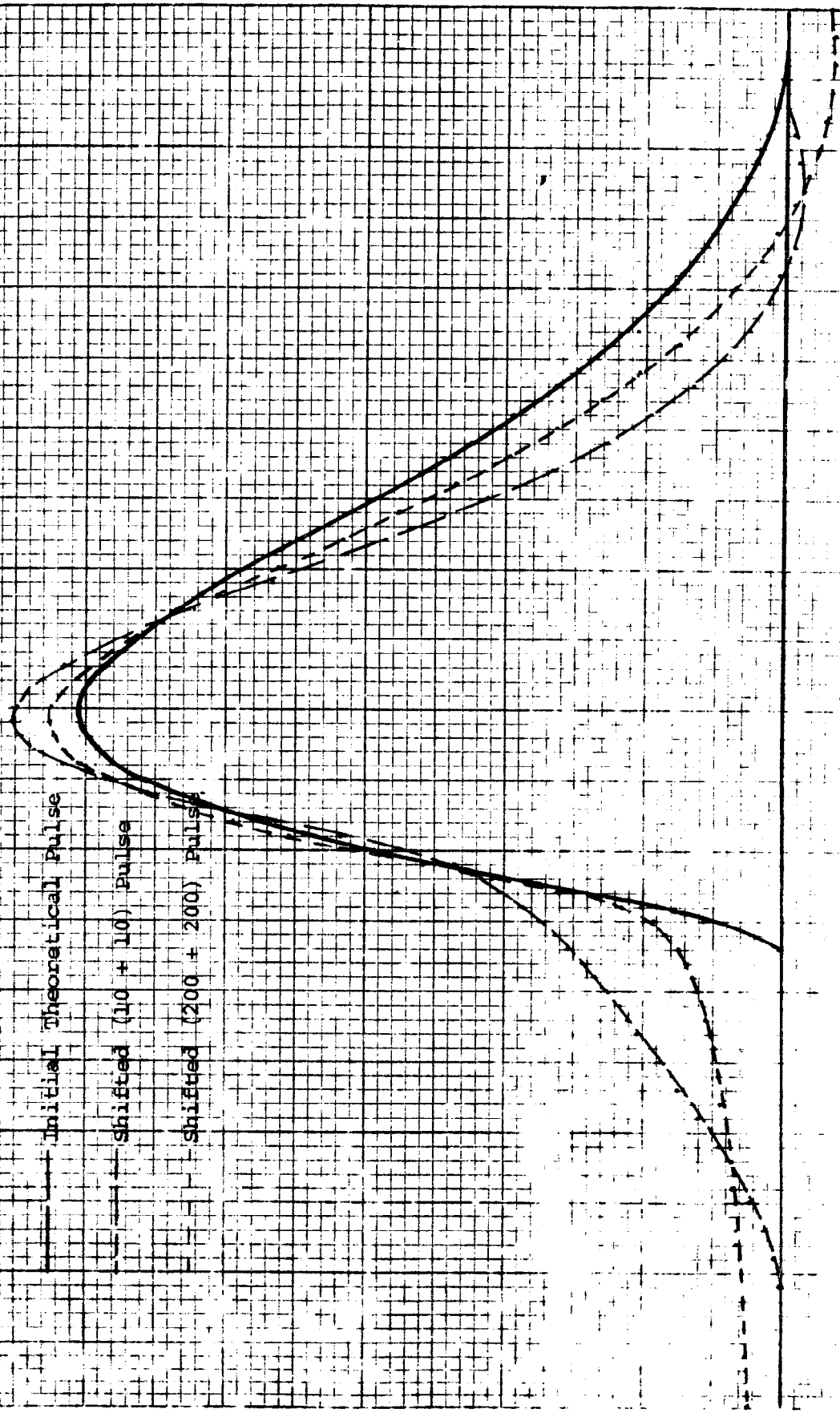


Fig. 4.5.3A. Effect of adding null signals of indicated duration (μsec) on computed shape of a distance-shifted theoretical impact pulse; only dispersion effects are considered.

THE INPUT FILNAME#R OUTPUTS: MAXIMUM NO. OF ENTRIES IN THE FILE= 100 PARAMETER RM =0.571F 10 BALL MASS= 0.280E 00
 SPEED OF SOUND IN THE BALL= 0.210E 00 INITIAL VELOCITY OF BALL= 0.174E 03 FINAL VELOCITY OF THE BALL= 0.154E 00
 VELOCITY OF THE BAR AFTER IMPACT= 0.651E 01 THE MASS OF THE BAR= 0.805E 03

TIME (SEC.)	DEPTH (MILS.)	PENETRATION VELOCITY (IN./SEC.)	FORCE (LBS.)	Pulse Energy	Local Energy	Total Energy	INSTANTANEOUS VELOCITY	REP MOMENTUM
0.	0.	0.174E 03	0.	0.	0.	0.	0.	0.
0.164E-05	0.114E 00	0.174E 03	0.786E 00	0.131E 00	0.502E 02	0.502E 02	0.174E 03	0.280E 00
0.331E-05	0.226E 00	0.172E 03	0.157E 01	0.286E 00	0.201F 03	0.201F 03	0.174E 03	0.114E 01
0.497E-05	0.339E 00	0.172E 03	0.255E 01	0.569E 01	0.664E 03	0.664E 03	0.174E 03	0.268E 01
0.663E-05	0.451E 00	0.172E 03	0.393E 01	0.785E 01	0.874E 03	0.874E 03	0.174E 03	0.504E 01
0.829E-05	0.563E 00	0.170E 03	0.549E 01	0.180E 02	0.149E 04	0.149E 04	0.174E 03	0.868E 01
0.994E-05	0.674E 00	0.169E 03	0.706E 01	0.450E 02	0.280E 04	0.280E 04	0.174E 03	0.134E 02
0.116E-04	0.783E 00	0.167E 03	0.119E 02	0.752E 02	0.346E 04	0.346E 04	0.174E 03	0.204E 02
0.133E-04	0.894E 00	0.165E 03	0.133E 02	0.144E 03	0.502E 04	0.502E 04	0.173E 03	0.276E 02
0.149E-04	0.998E 00	0.164E 03	0.157E 02	0.216E 03	0.677E 04	0.677E 04	0.173E 03	0.444E 02
0.166E-04	0.111E 01	0.160E 03	0.204E 02	0.376E 03	0.894E 04	0.894E 04	0.173E 03	0.627E 02
0.183E-04	0.120E 01	0.154E 03	0.304E 02	0.664E 03	0.119E 05	0.119E 05	0.172E 03	0.824E 02
0.213E-04	0.131E 01	0.150E 03	0.358E 02	0.113E 04	0.166E 05	0.166E 05	0.172E 03	0.944E 02
0.232E-04	0.140E 01	0.145E 03	0.428E 02	0.173F 04	0.215E 05	0.215E 05	0.171E 03	0.776E 02
0.249E-04	0.149E 01	0.139E 03	0.533E 02	0.276E 04	0.193E 05	0.193E 05	0.170E 03	0.120E 03
0.265E-04	0.158E 01	0.130E 03	0.633E 02	0.423E 04	0.248E 05	0.248E 05	0.169E 03	0.161E 03
0.282E-04	0.166E 01	0.125E 03	0.695E 02	0.610E 04	0.305E 05	0.305E 05	0.167E 03	0.204E 03
0.298E-04	0.175E 01	0.114E 03	0.848E 02	0.804E 04	0.365E 05	0.365E 05	0.165E 03	0.252E 03
0.315E-04	0.181E 01	0.103E 03	0.991E 02	0.122E 05	0.434E 05	0.434E 05	0.163E 03	0.308E 03
0.332E-04	0.194E 01	0.882E 02	0.108E 03	0.168E 05	0.508E 05	0.508E 05	0.161E 03	0.372E 03
0.348E-04	0.199E 01	0.792E 02	0.131E 03	0.221E 05	0.586E 05	0.586E 05	0.158E 03	0.445E 03
0.365E-04	0.204E 01	0.670E 02	0.141F 03	0.267E 05	0.661E 05	0.661E 05	0.155E 03	0.517E 03
0.381E-04	0.209E 01	0.580E 02	0.150E 03	0.454E 05	0.735E 05	0.735E 05	0.152E 03	0.627E 03
0.398E-04	0.212E 01	0.468E 02	0.163E 03	0.550E 05	0.806E 05	0.806E 05	0.149E 03	0.727E 03
0.414E-04	0.214E 01	0.383E 02	0.170E 03	0.677E 05	0.874E 05	0.874E 05	0.146E 03	0.834E 03
0.431E-04	0.217E 01	0.324F 02	0.172E 03	0.790F 05	0.935E 05	0.935E 05	0.143E 03	0.951E 03
0.447E-04	0.218E 01	0.227E 02	0.182E 03	0.915E 05	0.103E 06	0.103E 06	0.140E 03	0.107E 04
0.464E-04	0.220E 01	0.156E 02	0.185E 03	0.105E 05	0.106E 06	0.106E 06	0.137E 03	0.120E 04
0.481E-04	0.221E 01	0.977E 01	0.187E 03	0.122E 06	0.109E 06	0.109E 06	0.132E 03	0.133E 04
0.497E-04	0.220E 01	0.400E 01	0.188E 03	0.137E 06	0.109E 06	0.109E 06	0.122E 03	0.145E 04
0.514E-04	0.221E 01	-0.574E 00	0.188E 03	0.152F 06	0.111F 06	0.111F 06	0.117E 03	0.160E 04
0.530E-04	0.220E 01	-0.572E 01	0.188E 03	0.167F 06	0.111E 06	0.111E 06	0.112E 03	0.175E 04
0.547E-04	0.220E 01	-0.987E 01	0.187E 03	0.182E 06	0.110E 06	0.110E 06	0.109E 03	0.190E 04
0.563E-04	0.219E 01	-0.140E 02	0.186E 03	0.197E 06	0.109E 06	0.109E 06	0.102E 02	0.210E 04
0.580E-04	0.219E 01	-0.162E 02	0.182E 03	0.211F 06	0.106E 06	0.106E 06	0.893E 02	0.228E 04
0.597E-04	0.218E 01	-0.200E 02	0.180F 03	0.225E 06	0.106E 06	0.106E 06	0.852E 02	0.245E 04
0.613E-04	0.216E 01	-0.210E 02	0.176E 03	0.238E 06	0.106F 06	0.106F 06	0.810E 02	0.260E 04
0.630E-04	0.215E 01	-0.240F 02	0.174E 03	0.251F 06	0.974F 05	0.974F 05	0.762E 02	0.274E 04
0.646E-04	0.215E 01	-0.240E 02	0.165E 03	0.265E 06	0.955E 05	0.955E 05	0.708E 02	0.281E 04
0.663E-04	0.211E 01	-0.266E 02	0.161E 03	0.274E 06	0.925E 05	0.925E 05	0.650E 02	0.294E 04
0.679E-04	0.209E 01	-0.232E 02	0.144E 03	0.284E 06	0.876E 05	0.876E 05	0.601E 02	0.306E 04
0.696E-04	0.208E 01	-0.251E 02	0.144E 03	0.294E 06	0.827E 05	0.827E 05	0.550E 02	0.317E 04
0.712E-04	0.204E 01	-0.248E 02	0.135E 03	0.303E 06	0.778E 05	0.778E 05	0.500E 02	0.328E 04
0.729E-04	0.204E 01	-0.248E 02	0.131E 03	0.310E 06	0.734E 05	0.734E 05	0.454E 02	0.338E 04
0.746E-04	0.200E 01	-0.217E 02	0.123E 03	0.316E 06	0.701E 05	0.701E 05	0.408E 02	0.347E 04
0.779E-04	0.200E 01	-0.261E 02	0.114E 03	0.320E 06	0.673E 05	0.673E 05	0.375E 02	0.355E 04
0.795E-04	0.198E 01	-0.232E 02	0.114E 03	0.328E 06	0.645E 05	0.645E 05	0.348E 02	0.363E 04
0.812E-04	0.195E 01	-0.246E 02	0.105E 03	0.338E 06	0.617E 05	0.617E 05	0.321E 02	0.370E 04
0.828E-04	0.194E 01	-0.226E 02	0.104E 03	0.342E 06	0.590E 05	0.590E 05	0.295E 02	0.376E 04

Fig. 4.6A. Computer analysis of experimental pulse for GLIN-1.

U. 845E-04	0.194E 01	-0.205E 02	0.889E 02	0.345E 04	0.497E 05	0.415E 04	0.370E 02	0.404E 04
0.862E-04	0.191E 01	-0.207E 02	0.851E 02	0.340E 04	0.483E 05	0.417E 04	0.376E 02	0.417E 04
0.879E-04	0.190E 01	-0.171E 02	0.804E 02	0.330E 04	0.470E 05	0.420E 04	0.381E 02	0.419E 04
0.899E-04	0.188E 01	-0.181E 02	0.770E 02	0.356E 04	0.466E 05	0.420E 04	0.384E 02	0.424E 04
0.945E-04	0.188E 01	-0.181E 02	0.672E 02	0.350E 04	0.424E 05	0.431E 04	0.392E 02	0.433E 04
0.961E-04	0.185E 01	-0.177E 02	0.647E 02	0.362E 04	0.401E 05	0.424E 04	0.395E 02	0.438E 04
0.979E-04	0.182E 01	-0.184E 02	0.600E 02	0.362E 04	0.388E 05	0.424E 04	0.395E 02	0.443E 04
0.994E-04	0.180E 01	-0.161E 02	0.577E 02	0.366E 04	0.408E 05	0.425E 04	0.398E 02	0.448E 04
0.101E-03	0.180E 01	-0.162E 02	0.504E 02	0.366E 04	0.408E 05	0.425E 04	0.398E 02	0.448E 04
0.103E-03	0.183E 01	-0.165E 02	0.601E 02	0.360E 04	0.390E 05	0.427E 04	0.401E 02	0.453E 04
0.104E-03	0.177E 01	-0.172E 02	0.601E 02	0.360E 04	0.367E 05	0.426E 04	0.401E 02	0.455E 04
0.108E-03	0.172E 01	-0.164E 02	0.440E 02	0.360E 04	0.367E 05	0.426E 04	0.401E 02	0.455E 04
0.108E-03	0.178E 01	-0.169E 02	0.429E 02	0.369E 04	0.397E 05	0.429E 04	0.407E 02	0.467E 04
0.109E-03	0.177E 01	-0.170E 02	0.411E 02	0.373E 04	0.364E 05	0.429E 04	0.407E 02	0.470E 04
0.113E-03	0.177E 01	-0.155E 02	0.378E 02	0.373E 04	0.364E 05	0.429E 04	0.407E 02	0.470E 04
0.118E-03	0.173E 01	-0.169E 02	0.350E 02	0.373E 04	0.364E 05	0.429E 04	0.407E 02	0.470E 04
0.121E-03	0.170E 01	-0.167E 02	0.328E 02	0.373E 04	0.364E 05	0.429E 04	0.407E 02	0.470E 04
0.124E-03	0.167E 01	-0.166E 02	0.287E 02	0.376E 04	0.376E 05	0.430E 04	0.409E 02	0.470E 04
0.126E-03	0.166E 01	-0.172E 02	0.265E 02	0.376E 04	0.376E 05	0.430E 04	0.409E 02	0.470E 04
0.129E-03	0.168E 01	-0.171E 02	0.254E 02	0.376E 04	0.376E 05	0.430E 04	0.409E 02	0.470E 04
0.131E-03	0.162E 01	-0.168E 02	0.238E 02	0.376E 04	0.376E 05	0.430E 04	0.409E 02	0.470E 04
0.134E-03	0.162E 01	-0.197E 02	0.225E 02	0.376E 04	0.376E 05	0.430E 04	0.409E 02	0.470E 04
0.135E-03	0.163E 01	-0.170E 02	0.225E 02	0.376E 04	0.376E 05	0.430E 04	0.409E 02	0.470E 04
0.135E-03	0.158E 01	-0.184E 02	0.208E 02	0.376E 04	0.376E 05	0.430E 04	0.409E 02	0.470E 04
0.138E-03	0.162E 01	-0.165E 02	0.191E 02	0.376E 04	0.376E 05	0.430E 04	0.409E 02	0.470E 04
0.138E-03	0.162E 01	-0.162E 02	0.179E 02	0.376E 04	0.376E 05	0.430E 04	0.409E 02	0.470E 04
0.139E-03	0.154E 01	-0.165E 02	0.173E 02	0.376E 04	0.376E 05	0.430E 04	0.409E 02	0.470E 04
0.141E-03	0.157E 01	-0.157E 02	0.159E 02	0.376E 04	0.376E 05	0.430E 04	0.409E 02	0.470E 04
0.142E-03	0.151E 01	-0.157E 02	0.149E 02	0.376E 04	0.376E 05	0.430E 04	0.409E 02	0.470E 04
0.144E-03	0.153E 01	-0.154E 02	0.142E 02	0.376E 04	0.376E 05	0.430E 04	0.409E 02	0.470E 04
0.146E-03	0.155E 01	-0.150E 02	0.128E 02	0.376E 04	0.376E 05	0.430E 04	0.409E 02	0.470E 04
0.148E-03	0.155E 01	-0.150E 02	0.118E 02	0.376E 04	0.376E 05	0.430E 04	0.409E 02	0.470E 04
0.149E-03	0.150E 01	-0.148E 02	0.111E 02	0.376E 04	0.376E 05	0.430E 04	0.409E 02	0.470E 04
0.151E-03	0.152E 01	-0.151E 02	0.110E 02	0.376E 04	0.376E 05	0.430E 04	0.409E 02	0.470E 04
0.152E-03	0.145E 01	-0.147E 02	0.102E 02	0.376E 04	0.376E 05	0.430E 04	0.409E 02	0.470E 04
0.154E-03	0.149E 01	-0.147E 02	0.924E 01	0.370E 06	0.471E 05	0.427E 04	0.417E 04	0.517E 04
0.158E-03	0.142E 01	-0.144E 02	0.768E 01	0.370E 06	0.480E 05	0.427E 04	0.417E 04	0.517E 04
0.159E-03	0.144E 01	-0.141E 02	0.728E 01	0.370E 06	0.481E 05	0.427E 04	0.417E 04	0.517E 04
0.161E-03	0.147E 01	-0.137E 02	0.647E 01	0.370E 06	0.472E 05	0.427E 04	0.417E 04	0.517E 04
0.162E-03	0.159E 01	-0.137E 02	0.549E 01	0.370E 06	0.490E 05	0.428E 04	0.418E 04	0.522E 04
0.165E-03	0.144E 01	-0.131E 02	0.451E 01	0.370E 06	0.481E 05	0.427E 04	0.418E 04	0.522E 04
0.167E-03	0.138E 01	-0.130E 02	0.433E 01	0.370E 06	0.472E 05	0.427E 04	0.418E 04	0.522E 04
0.169E-03	0.140E 01	-0.124E 02	0.335E 01	0.370E 06	0.472E 05	0.427E 04	0.418E 04	0.522E 04
0.171E-03	0.140E 01	-0.122E 02	0.293E 01	0.370E 06	0.463E 05	0.426E 04	0.418E 04	0.522E 04
0.172E-03	0.135E 01	-0.128E 02	0.205E 01	0.370E 06	0.463E 05	0.426E 04	0.418E 04	0.522E 04
0.174E-03	0.138E 01	-0.127E 02	0.275E 01	0.370E 06	0.482E 05	0.427E 04	0.418E 04	0.522E 04
0.176E-03	0.140E 01	-0.124E 02	0.236E 01	0.370E 06	0.482E 05	0.427E 04	0.418E 04	0.522E 04
0.177E-03	0.135E 01	-0.123E 02	0.216E 01	0.370E 06	0.472E 05	0.427E 04	0.418E 04	0.522E 04
0.179E-03	0.136E 01	-0.123E 02	0.214E 01	0.370E 06	0.472E 05	0.427E 04	0.418E 04	0.522E 04
0.181E-03	0.132E 01	-0.121E 02	0.177E 01	0.370E 06	0.472E 05	0.427E 04	0.418E 04	0.522E 04
0.182E-03	0.132E 01	-0.121E 02	0.177E 01	0.370E 06	0.463E 05	0.426E 04	0.418E 04	0.522E 04
0.184E-03	0.134E 01	-0.119E 02	0.138E 01	0.370E 06	0.463E 05	0.426E 04	0.418E 04	0.522E 04
0.185E-03	0.130E 01	-0.114E 02	0.119E 01	0.370E 06	0.463E 05	0.426E 04	0.418E 04	0.522E 04
0.187E-03	0.130E 01	-0.114E 02	0.992E 00	0.370E 06	0.463E 05	0.426E 04	0.418E 04	0.522E 04
0.189E-03	0.132E 01	-0.116E 02	0.982E 00	0.370E 06	0.463E 05	0.426E 04	0.418E 04	0.522E 04
0.191E-03	0.133E 01	-0.116E 02	0.982E 00	0.370E 06	0.463E 05	0.426E 04	0.418E 04	0.522E 04
0.192E-03	0.127E 01	-0.122E 02	0.982E 00	0.370E 06	0.463E 05	0.426E 04	0.418E 04	0.522E 04
0.194E-03	0.128E 01	-0.122E 02	0.982E 00	0.370E 06	0.463E 05	0.426E 04	0.418E 04	0.522E 04
0.196E-03	0.130E 01	-0.121E 02	0.786E 00	0.370E 06	0.463E 05	0.426E 04	0.418E 04	0.522E 04
0.197E-03	0.126E 01	-0.121E 02	0.786E 00	0.370E 06	0.463E 05	0.426E 04	0.418E 04	0.522E 04
0.199E-03	0.126E 01	-0.121E 02	0.786E 00	0.370E 06	0.463E 05	0.426E 04	0.418E 04	0.522E 04
0.201E-03	0.128E 01	-0.121E 02	0.786E 00	0.370E 06	0.463E 05	0.426E 04	0.418E 04	0.522E 04
0.202E-03	0.122E 01	-0.121E 02	0.786E 00	0.370E 06	0.463E 05	0.426E 04	0.418E 04	0.522E 04

Fig. 4.6A, cont'd.

BEST AVAILABLE COPY

***EXPERIMENTAL IDENTIFICATION** > (CROSS-SECTION) CALC. ON GLIN-1 (3)

THE INPUT FILENAME OUTDUSTS: MAXIMUM NO. OF ENTRIES IN THE FILE IS PROHIBITED BE $0.6642E+06$ BALL MASS $0.2487E+02$
 SPEED OF SOUND IN THE MEDIUM: MAXIMUM INITIAL VELOCITY OF BALL $0.174E+03$ FINAL VELOCITY OF THE BALL $0.174E+02$
 VELOCITY OF THE RAD AFTER IMPACT $0.673E+01$ THE MASS OF THE GASE $0.800E+01$

TIME (SEC.)	DEPTH (MILS.)	PENETRATION VELOCITY (IN./SEC.)	FORCE (LBS.)	Pulse Energy	Local Energy	Total Energy	INSTANTANEOUS VELOCITY	QAR MOMENTUM
0.	0.	0.174E+03	0.	0.	0.	0.	0.	0.
0.100E-05	0.641E-01	0.172E+03	0.477E+01	0.155E+01	0.143E+03	0.144E+03	0.174E+02	0.1420E+01
0.200E-05	0.115E+00	0.168E+03	0.104E+02	0.151E+02	0.609E+03	0.609E+03	0.174E+02	0.170E+01
0.300E-05	0.201E+00	0.164E+03	0.100E+02	0.640E+02	0.187E+04	0.187E+04	0.174E+02	0.195E+02
0.400E-05	0.264E+00	0.159E+03	0.287E+02	0.197E+03	0.366E+04	0.366E+04	0.173E+02	0.211E+02
0.500E-05	0.326E+00	0.151E+03	0.504E+02	0.657E+03	0.588E+04	0.620E+04	0.172E+02	0.216E+02
0.600E-05	0.388E+00	0.142E+03	0.508E+02	0.910E+03	0.881E+04	0.972E+04	0.172E+02	0.216E+02
0.700E-05	0.448E+00	0.133E+03	0.927E+02	0.167E+04	0.124E+05	0.140E+05	0.171E+02	0.216E+02
0.800E-05	0.508E+00	0.124E+03	0.850E+02	0.265E+04	0.165E+05	0.182E+05	0.170E+02	0.216E+02
0.900E-05	0.568E+00	0.115E+03	0.977E+02	0.426E+04	0.213E+05	0.232E+05	0.169E+02	0.216E+02
0.100E-04	0.640E+00	0.112E+03	0.100E+03	0.831E+04	0.261E+05	0.281E+05	0.168E+02	0.216E+02
0.120E-04	0.682E+00	0.104E+03	0.121E+03	0.112E+05	0.316E+05	0.336E+05	0.166E+02	0.216E+02
0.130E-04	0.723E+00	0.970E+02	0.131E+03	0.147E+05	0.370E+05	0.488E+05	0.164E+02	0.216E+02
0.140E-04	0.759E+00	0.809E+02	0.141E+03	0.198E+05	0.424E+05	0.531E+05	0.162E+02	0.216E+02
0.150E-04	0.795E+00	0.827E+02	0.151E+03	0.255E+05	0.487E+05	0.621E+05	0.160E+02	0.216E+02
0.160E-04	0.824E+00	0.757E+02	0.160E+03	0.288E+05	0.558E+05	0.728E+05	0.158E+02	0.216E+02
0.170E-04	0.852E+00	0.699E+02	0.160E+03	0.348E+05	0.646E+05	0.802E+05	0.157E+02	0.216E+02
0.180E-04	0.879E+00	0.634E+02	0.176E+03	0.348E+05	0.697E+05	0.802E+05	0.157E+02	0.216E+02
0.190E-04	0.902E+00	0.560E+02	0.184E+03	0.444E+05	0.743E+05	0.121E+06	0.157E+02	0.216E+02
0.200E-04	0.923E+00	0.500E+02	0.190E+03	0.563E+05	0.785E+05	0.135E+06	0.156E+02	0.216E+02
0.210E-04	0.947E+00	0.440E+02	0.196E+03	0.647E+05	0.829E+05	0.147E+06	0.154E+02	0.216E+02
0.220E-04	0.957E+00	0.384E+02	0.201E+03	0.728E+05	0.866E+05	0.159E+06	0.153E+02	0.216E+02
0.230E-04	0.971E+00	0.320E+02	0.206E+03	0.810E+05	0.899E+05	0.172E+06	0.151E+02	0.216E+02
0.240E-04	0.985E+00	0.257E+02	0.209E+03	0.914E+05	0.926E+05	0.184E+06	0.149E+02	0.216E+02
0.250E-04	0.998E+00	0.220E+02	0.212E+03	0.101E+06	0.950E+05	0.194E+06	0.147E+02	0.216E+02
0.260E-04	0.101E+01	0.132E+02	0.215E+03	0.111E+06	0.966E+05	0.208E+06	0.145E+02	0.216E+02
0.270E-04	0.102E+01	0.132E+02	0.217E+03	0.122E+06	0.981E+05	0.220E+06	0.143E+02	0.216E+02
0.280E-04	0.101E+01	0.964E+01	0.210E+03	0.132E+06	0.981E+05	0.232E+06	0.141E+02	0.216E+02
0.290E-04	0.102E+01	0.574E+01	0.220E+03	0.142E+06	0.100E+06	0.244E+06	0.139E+02	0.216E+02
0.300E-04	0.102E+01	0.189E+01	0.220E+03	0.151E+06	0.101E+06	0.254E+06	0.137E+02	0.216E+02
0.310E-04	0.102E+01	-0.157E+01	0.220E+03	0.164E+06	0.100E+06	0.264E+06	0.135E+02	0.216E+02
0.320E-04	0.102E+01	-0.468E+01	0.220E+03	0.175E+06	0.100E+06	0.274E+06	0.133E+02	0.216E+02
0.330E-04	0.102E+01	-0.759E+01	0.210E+03	0.185E+06	0.983E+05	0.284E+06	0.131E+02	0.216E+02
0.340E-04	0.101E+01	-1.109E+01	0.218E+03	0.196E+06	0.983E+05	0.294E+06	0.129E+02	0.216E+02
0.350E-04	0.100E+01	-1.434E+01	0.214E+03	0.206E+06	0.985E+05	0.304E+06	0.127E+02	0.216E+02
0.360E-04	0.998E+00	-1.759E+01	0.214E+03	0.216E+06	0.972E+05	0.314E+06	0.125E+02	0.216E+02
0.370E-04	0.995E+00	-2.082E+01	0.212E+03	0.226E+06	0.957E+05	0.324E+06	0.123E+02	0.216E+02
0.380E-04	0.993E+00	-2.402E+01	0.210E+03	0.236E+06	0.936E+05	0.334E+06	0.121E+02	0.216E+02
0.390E-04	0.973E+00	-2.722E+01	0.207E+03	0.246E+06	0.916E+05	0.344E+06	0.119E+02	0.216E+02
0.400E-04	0.973E+00	-3.042E+01	0.204E+03	0.256E+06	0.897E+05	0.354E+06	0.117E+02	0.216E+02
0.410E-04	0.950E+00	-3.362E+01	0.201E+03	0.266E+06	0.880E+05	0.364E+06	0.115E+02	0.216E+02
0.420E-04	0.948E+00	-3.682E+01	0.198E+03	0.276E+06	0.853E+05	0.374E+06	0.113E+02	0.216E+02
0.430E-04	0.940E+00	-4.002E+01	0.195E+03	0.286E+06	0.823E+05	0.384E+06	0.111E+02	0.216E+02
0.440E-04	0.927E+00	-4.321E+01	0.191E+03	0.296E+06	0.784E+05	0.394E+06	0.109E+02	0.216E+02
0.450E-04	0.912E+00	-4.641E+01	0.187E+03	0.306E+06	0.745E+05	0.404E+06	0.107E+02	0.216E+02
0.460E-04	0.902E+00	-4.961E+01	0.184E+03	0.316E+06	0.706E+05	0.414E+06	0.105E+02	0.216E+02
0.470E-04	0.892E+00	-5.281E+01	0.180E+03	0.326E+06	0.667E+05	0.424E+06	0.103E+02	0.216E+02
0.480E-04	0.879E+00	-5.601E+01	0.174E+03	0.336E+06	0.628E+05	0.434E+06	0.101E+02	0.216E+02
0.490E-04	0.866E+00	-5.921E+01	0.171E+03	0.346E+06	0.589E+05	0.444E+06	0.099E+02	0.216E+02

Fig. 4.6B. Computer analysis of theoretical pulse for GLIN-1.

BEST AVAILABLE COPY

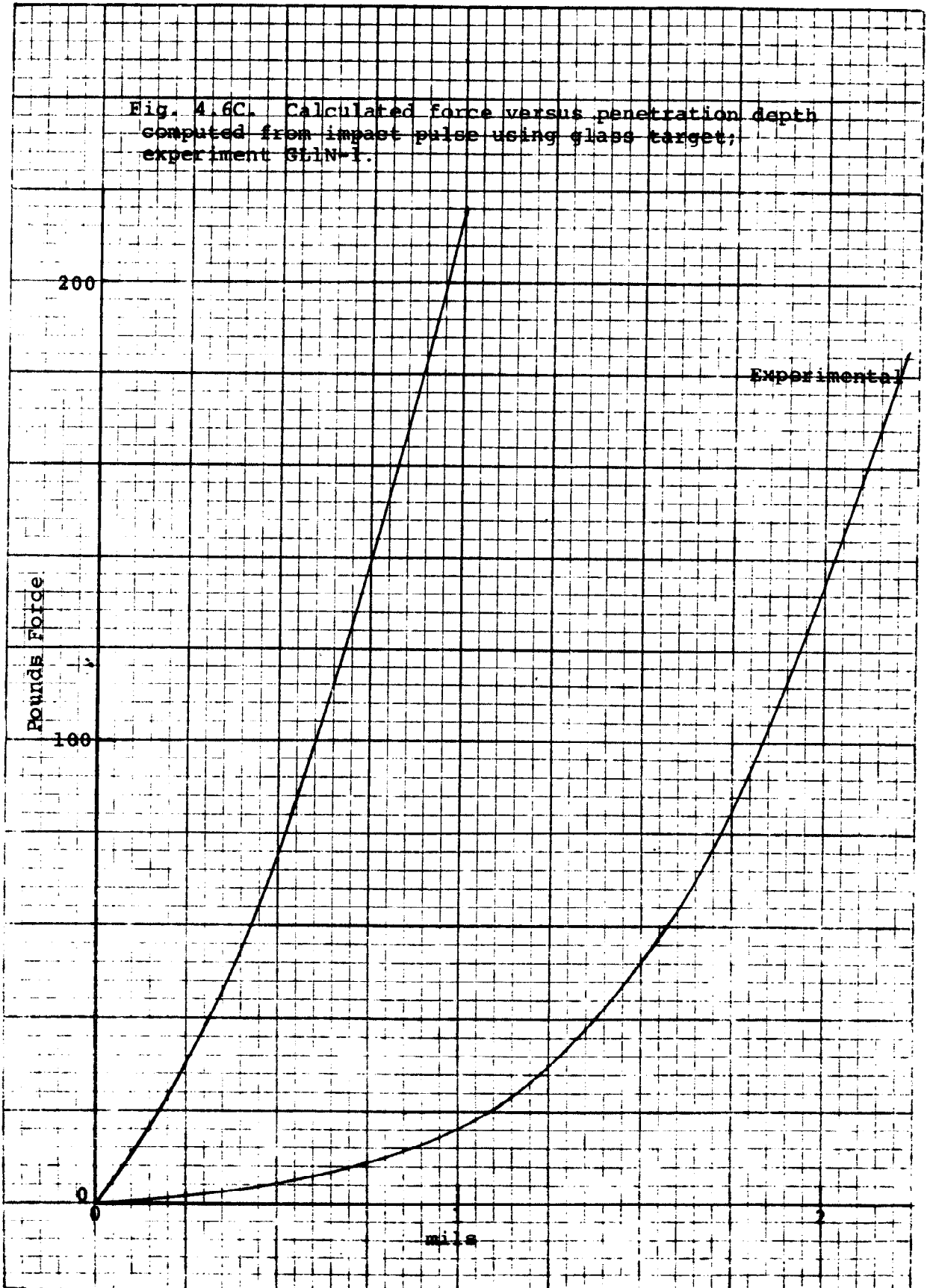
0.500E-04	0.864E 00	-0.357E 03	0.147E 07	0.832E 04	0.647E 06	1.707E 04	0.478E 03	0.557E 04
0.510E-04	0.875E 00	-0.357E 03	0.148E 07	0.838E 04	0.650E 06	1.707E 04	0.483E 03	0.567E 04
0.520E-04	0.887E 00	-0.356E 03	0.149E 07	0.844E 04	0.653E 06	1.707E 04	0.488E 03	0.577E 04
0.530E-04	0.899E 00	-0.356E 03	0.150E 07	0.850E 04	0.656E 06	1.707E 04	0.493E 03	0.587E 04
0.540E-04	0.911E 00	-0.355E 03	0.151E 07	0.856E 04	0.659E 06	1.707E 04	0.498E 03	0.597E 04
0.550E-04	0.923E 00	-0.354E 03	0.152E 07	0.862E 04	0.662E 06	1.707E 04	0.503E 03	0.607E 04
0.560E-04	0.935E 00	-0.353E 03	0.153E 07	0.868E 04	0.665E 06	1.707E 04	0.508E 03	0.617E 04
0.570E-04	0.947E 00	-0.352E 03	0.154E 07	0.874E 04	0.668E 06	1.707E 04	0.513E 03	0.627E 04
0.580E-04	0.959E 00	-0.351E 03	0.155E 07	0.880E 04	0.671E 06	1.707E 04	0.518E 03	0.637E 04
0.590E-04	0.971E 00	-0.350E 03	0.156E 07	0.886E 04	0.674E 06	1.707E 04	0.523E 03	0.647E 04
0.600E-04	0.983E 00	-0.349E 03	0.157E 07	0.892E 04	0.677E 06	1.707E 04	0.528E 03	0.657E 04
0.610E-04	0.995E 00	-0.348E 03	0.158E 07	0.898E 04	0.680E 06	1.707E 04	0.533E 03	0.667E 04
0.620E-04	1.007E 00	-0.347E 03	0.159E 07	0.904E 04	0.683E 06	1.707E 04	0.538E 03	0.677E 04
0.630E-04	1.019E 00	-0.346E 03	0.160E 07	0.910E 04	0.686E 06	1.707E 04	0.543E 03	0.687E 04
0.640E-04	1.031E 00	-0.345E 03	0.161E 07	0.916E 04	0.689E 06	1.707E 04	0.548E 03	0.697E 04
0.650E-04	1.043E 00	-0.344E 03	0.162E 07	0.922E 04	0.692E 06	1.707E 04	0.553E 03	0.707E 04
0.660E-04	1.055E 00	-0.343E 03	0.163E 07	0.928E 04	0.695E 06	1.707E 04	0.558E 03	0.717E 04
0.670E-04	1.067E 00	-0.342E 03	0.164E 07	0.934E 04	0.698E 06	1.707E 04	0.563E 03	0.727E 04
0.680E-04	1.079E 00	-0.341E 03	0.165E 07	0.940E 04	0.701E 06	1.707E 04	0.568E 03	0.737E 04
0.690E-04	1.091E 00	-0.340E 03	0.166E 07	0.946E 04	0.704E 06	1.707E 04	0.573E 03	0.747E 04
0.700E-04	1.103E 00	-0.339E 03	0.167E 07	0.952E 04	0.707E 06	1.707E 04	0.578E 03	0.757E 04
0.710E-04	1.115E 00	-0.338E 03	0.168E 07	0.958E 04	0.710E 06	1.707E 04	0.583E 03	0.767E 04
0.720E-04	1.127E 00	-0.337E 03	0.169E 07	0.964E 04	0.713E 06	1.707E 04	0.588E 03	0.777E 04
0.730E-04	1.139E 00	-0.336E 03	0.170E 07	0.970E 04	0.716E 06	1.707E 04	0.593E 03	0.787E 04
0.740E-04	1.151E 00	-0.335E 03	0.171E 07	0.976E 04	0.719E 06	1.707E 04	0.598E 03	0.797E 04
0.750E-04	1.163E 00	-0.334E 03	0.172E 07	0.982E 04	0.722E 06	1.707E 04	0.603E 03	0.807E 04
0.760E-04	1.175E 00	-0.333E 03	0.173E 07	0.988E 04	0.725E 06	1.707E 04	0.608E 03	0.817E 04
0.770E-04	1.187E 00	-0.332E 03	0.174E 07	0.994E 04	0.728E 06	1.707E 04	0.613E 03	0.827E 04
0.780E-04	1.199E 00	-0.331E 03	0.175E 07	1.000E 04	0.731E 06	1.707E 04	0.618E 03	0.837E 04
0.790E-04	1.211E 00	-0.330E 03	0.176E 07	1.006E 04	0.734E 06	1.707E 04	0.623E 03	0.847E 04
0.800E-04	1.223E 00	-0.329E 03	0.177E 07	1.012E 04	0.737E 06	1.707E 04	0.628E 03	0.857E 04
0.810E-04	1.235E 00	-0.328E 03	0.178E 07	1.018E 04	0.740E 06	1.707E 04	0.633E 03	0.867E 04
0.820E-04	1.247E 00	-0.327E 03	0.179E 07	1.024E 04	0.743E 06	1.707E 04	0.638E 03	0.877E 04
0.830E-04	1.259E 00	-0.326E 03	0.180E 07	1.030E 04	0.746E 06	1.707E 04	0.643E 03	0.887E 04
0.840E-04	1.271E 00	-0.325E 03	0.181E 07	1.036E 04	0.749E 06	1.707E 04	0.648E 03	0.897E 04
0.850E-04	1.283E 00	-0.324E 03	0.182E 07	1.042E 04	0.752E 06	1.707E 04	0.653E 03	0.907E 04
0.860E-04	1.295E 00	-0.323E 03	0.183E 07	1.048E 04	0.755E 06	1.707E 04	0.658E 03	0.917E 04
0.870E-04	1.307E 00	-0.322E 03	0.184E 07	1.054E 04	0.758E 06	1.707E 04	0.663E 03	0.927E 04
0.880E-04	1.319E 00	-0.321E 03	0.185E 07	1.060E 04	0.761E 06	1.707E 04	0.668E 03	0.937E 04
0.890E-04	1.331E 00	-0.320E 03	0.186E 07	1.066E 04	0.764E 06	1.707E 04	0.673E 03	0.947E 04
0.900E-04	1.343E 00	-0.319E 03	0.187E 07	1.072E 04	0.767E 06	1.707E 04	0.678E 03	0.957E 04
0.910E-04	1.355E 00	-0.318E 03	0.188E 07	1.078E 04	0.770E 06	1.707E 04	0.683E 03	0.967E 04
0.920E-04	1.367E 00	-0.317E 03	0.189E 07	1.084E 04	0.773E 06	1.707E 04	0.688E 03	0.977E 04
0.930E-04	1.379E 00	-0.316E 03	0.190E 07	1.090E 04	0.776E 06	1.707E 04	0.693E 03	0.987E 04
0.940E-04	1.391E 00	-0.315E 03	0.191E 07	1.096E 04	0.779E 06	1.707E 04	0.698E 03	0.997E 04
0.950E-04	1.403E 00	-0.314E 03	0.192E 07	1.102E 04	0.782E 06	1.707E 04	0.703E 03	1.007E 04
0.960E-04	1.415E 00	-0.313E 03	0.193E 07	1.108E 04	0.785E 06	1.707E 04	0.708E 03	1.017E 04
0.970E-04	1.427E 00	-0.312E 03	0.194E 07	1.114E 04	0.788E 06	1.707E 04	0.713E 03	1.027E 04
0.980E-04	1.439E 00	-0.311E 03	0.195E 07	1.120E 04	0.791E 06	1.707E 04	0.718E 03	1.037E 04
0.990E-04	1.451E 00	-0.310E 03	0.196E 07	1.126E 04	0.794E 06	1.707E 04	0.723E 03	1.047E 04
1.000E-04	1.463E 00	-0.309E 03	0.197E 07	1.132E 04	0.797E 06	1.707E 04	0.728E 03	1.057E 04
0.995E-04	1.475E 00	-0.308E 03	0.198E 07	1.138E 04	0.800E 06	1.707E 04	0.733E 03	1.067E 04
0.990E-04	1.487E 00	-0.307E 03	0.199E 07	1.144E 04	0.803E 06	1.707E 04	0.738E 03	1.077E 04
0.985E-04	1.499E 00	-0.306E 03	0.200E 07	1.150E 04	0.806E 06	1.707E 04	0.743E 03	1.087E 04
0.980E-04	1.511E 00	-0.305E 03	0.201E 07	1.156E 04	0.809E 06	1.707E 04	0.748E 03	1.097E 04
0.975E-04	1.523E 00	-0.304E 03	0.202E 07	1.162E 04	0.812E 06	1.707E 04	0.753E 03	1.107E 04
0.970E-04	1.535E 00	-0.303E 03	0.203E 07	1.168E 04	0.815E 06	1.707E 04	0.758E 03	1.117E 04
0.965E-04	1.547E 00	-0.302E 03	0.204E 07	1.174E 04	0.818E 06	1.707E 04	0.763E 03	1.127E 04
0.960E-04	1.559E 00	-0.301E 03	0.205E 07	1.180E 04	0.821E 06	1.707E 04	0.768E 03	1.137E 04
0.955E-04	1.571E 00	-0.300E 03	0.206E 07	1.186E 04	0.824E 06	1.707E 04	0.773E 03	1.147E 04
0.950E-04	1.583E 00	-0.299E 03	0.207E 07	1.192E 04	0.827E 06	1.707E 04	0.778E 03	1.157E 04
0.945E-04	1.595E 00	-0.298E 03	0.208E 07	1.198E 04	0.830E 06	1.707E 04	0.783E 03	1.167E 04
0.940E-04	1.607E 00	-0.297E 03	0.209E 07	1.204E 04	0.833E 06	1.707E 04	0.788E 03	1.177E 04
0.935E-04	1.619E 00	-0.296E 03	0.210E 07	1.210E 04	0.836E 06	1.707E 04	0.793E 03	1.187E 04
0.930E-04	1.631E 00	-0.295E 03	0.211E 07	1.216E 04	0.839E 06	1.707E 04	0.798E 03	1.197E 04
0.925E-04	1.643E 00	-0.294E 03	0.212E 07	1.222E 04	0.842E 06	1.707E 04	0.803E 03	1.207E 04
0.920E-04	1.655E 00	-0.293E 03	0.213E 07	1.228E 04	0.845E 06	1.707E 04	0.808E 03	1.217E 04
0.915E-04	1.667E 00	-0.292E 03	0.214E 07	1.234E 04	0.848E 06	1.707E 04	0.813E 03	1.227E 04
0.910E-04	1.679E 00	-0.291E 03	0.215E 07	1.240E 04	0.851E 06	1.707E 04	0.818E 03	1.237E 04
0.905E-04	1.691E 00	-0.290E 03	0.216E 07	1.246E 04	0.854E 06	1.707E 04	0.823E 03	1.247E 04
0.900E-04	1.703E 00	-0.289E 03	0.217E 07	1.252E 04	0.857E 06	1.707E 04	0.828E 03	1.257E 04
0.895E-04	1.715E 00	-0.288E 03	0.218E 07	1.258E 04	0.860E 06	1.707E 04	0.833E 03	1.267E 04
0.890E-04	1.727E 00	-0.287E 03	0.219E 07	1.264E 04	0.863E 06	1.707E 04	0.838E 03	1.277E 04
0.885E-04	1.739E 00	-0.286E 03	0.220E 07	1.270E 04	0.866E 06	1.707E 04	0.843E 03	1.287E 04
0.880E-04	1.751E 00	-0.285E 03	0.221E 07	1.276E 04	0.869E 06	1.707E 04	0.848E 03	1.297E 04
0.875E-04	1.763E 00	-0.284E 03	0.222E 07	1.282E 04	0.872E 06	1.707E 04	0.853E 03	1.307E 04
0.870E-04	1.775E 00	-0.283E 03	0.223E 07	1.288E 04	0.875E 06	1.707E 04	0.858E 03	1.317E 04
0.865E-04	1.787E 00	-0.282E 03	0.224E 07	1.294E 04	0.878E 06	1.707E 04	0.863E 03	1.327E 04
0.860E-04	1.799E 00	-0.281E 03	0.225E 07	1.300E 04	0.881E 06	1.707E 04	0.868E 03	1.337E 04
0.855E-04	1.811E 00	-0.280E 03	0.226E 07	1.306E 04	0.884E 06	1.707E 04	0.873E 03	1.347E 04
0.850E-04	1.823E 00	-0.279E 03	0.227E 07	1.312E 04	0.887E 06	1.707E 04	0.878E 03	1.357E 04
0.845E-04	1.835E 00	-0.278E 03	0.228E 07	1.318E 04	0.890E 06	1.707E 04	0.883E 03	1.367E 04
0.840E-04	1.847E 00	-0.277E 03	0.229E 07	1.324E 04	0.893E 06	1.707E 04	0.888E 03	1.377E 04
0.835E-04	1.859E 00	-0.276E 03	0.230E 07	1.330E 04	0.896E 06	1.707E 04	0.893E 03	1.387E 04
0.830E-04	1.871E 00	-0.275E 03	0.231E 07	1.336E 04	0.899E 06	1.707E 04	0.898E 03	1.397E 04
0.825E-04	1.883E 00	-0.274E 03	0.232E 07	1.342E 04	0.902E 06	1.707E 04	0.903E 03	1.407E 04
0.820E-04	1.895E 00	-0.273E 03	0.233E 07	1.348E 04	0.905E 06	1.707E 04	0.908E 03	1.417E 04
0.815E-04	1.907E 00	-0.272E 03	0.234E 07	1.354E 04	0.908E 06	1.707E 04	0.913E 03	1.427E 04
0.810E-04	1.919E 00	-0.271E 03	0.235E 07	1.360E 04	0.911E 06	1.707E 04	0.918E 03	1.437E 04
0.805E-04	1.931E 00	-0.270E 03	0.236E 07	1.366E 04	0.914E 06	1.707E 04	0.923E 03	1.447E 04
0.800E-04	1.943E 00	-0.269E 03	0.237E 07	1.372E 04	0.917E 06	1.707E 04	0.928E 03	1.457E 04
0.795E-04	1.955E 00	-0.268E 03	0.238E 07	1.378E 04	0.920E 06	1.707E 04	0.933E 03	1.467E 04
0.790E-04	1.967E 00	-0.267E 03	0.239E 07	1.384E 04	0.923E 06	1.707E 04	0.938E 03	1.477E 04
0.785E-04	1.979E 00	-0.266E 03	0.240E 07	1.390E 04	0.926E 06	1.707E 04	0.943E 03	1.487E 04
0.780E-04	1.991E 00	-						

BEST AVAILABLE COPY

0.114E-03	0.708E-01	-0.100E	0.832E 01	0.425E 04	-0.165E 04	0.474E 04	0.173E 02	0.541E 04
0.117E-03	0.698E-01	-0.187E	0.704E 01	0.425E 04	-0.270E 04	0.423E 04	-0.173E 02	0.541E 04
0.118E-03	0.500E-01	-0.185E	0.235E 01	0.425E 04	-0.270E 04	0.423E 04	-0.173E 02	0.541E 04
0.119E-03	0.500E-01	-0.185E	0.180E 01	0.425E 04	-0.270E 04	0.423E 04	-0.173E 02	0.541E 04
0.120E-03	0.601E-01	-0.180E	0.346E 01	0.425E 04	-0.270E 04	0.423E 04	-0.173E 02	0.541E 04
0.121E-03	0.301E-01	-0.178E	0.108E 01	0.425E 04	-0.270E 04	0.423E 04	-0.173E 02	0.541E 04
0.122E-03	0.120E-01	-0.183E	0.677E 00	0.425E 04	-0.270E 04	0.423E 04	-0.173E 02	0.541E 04
0.123E-03	0.202E-02	-0.181E	0.878E 00	0.425E 04	-0.270E 04	0.423E 04	-0.173E 02	0.541E 04
0.124E-03	0.202E-02	-0.180E	0.115E 00	0.425E 04	-0.270E 04	0.423E 04	-0.173E 02	0.541E 04
0.	0.867E 00	-0.173E	0.	0.425E 04	-0.270E 04	0.423E 04	-0.173E 02	0.541E 04
0.	0.867E 00	-0.173E	0.	0.425E 04	-0.270E 04	0.423E 04	-0.173E 02	0.541E 04
0.	0.867E 00	-0.173E	0.	0.425E 04	-0.270E 04	0.423E 04	-0.173E 02	0.541E 04
0.	0.867E 00	-0.173E	0.	0.425E 04	-0.270E 04	0.423E 04	-0.173E 02	0.541E 04
0.	0.867E 00	-0.173E	0.	0.425E 04	-0.270E 04	0.423E 04	-0.173E 02	0.541E 04

Fig. 4.6B, cont'd.

Fig. 4.6C. Calculated force versus penetration depth computed from impact pulse using glass target; experiment 611N-1.



DISTRIBUTION LIST

Contract No. N00019-76-C-0330

Naval Air Systems Command Attn: Code AIR-52032 Washington, DC 20361	14	Air Force Materials Laboratory Wright-Patterson Air Force Base Dayton, OH 45433 Attn: LN 1 LAE 1	9
Naval Air Systems Command Attn: Code AIR-604 Washington, DC 20361	12	LNC 1 MX 1 LNE 1 LY 1 LNP 1 LT 1 MBC 1 (T. J. Reinhart)	
Office of Naval Research Washington, DC 20361 Attn: Code 471 Code 472 Code 473	3	Naval Research Laboratory Washington, DC 20390 Attn: Code 6000 Code 6100 Code 8433	3
Naval Ordnance Laboratory White Oak, MD 20910 Attn: Code 2301 Code 234	2	Atomic Energy Commission Technical Information Service P. O. Box 62 Oak Ridge, TN 37830	1
Materials Sciences & Engineering Laboratory Stanford Research Institute Menlo Park, CA 94025	1	NASA Headquarters Attn: B. G. Achhammer Washington, DC 20546	1
Institute for Materials Research National Bureau of Standards Washington, DC 20234	3	NASA-Lewis Research Center Attn: R. F. Lark, Mail Stop 49-1 21000 Brookpark Road Cleveland, OH 44135	1
Battelle Memorial Institute 505 King Avenue Columbus, OH 43201	1	Army Materials & Mechanics Research Center Watertown, MA 02172 Attn: Dr. R. N. Katz Dr. G. Thomas Dr. R. Lewis	3
IIT Research Institute Attn: Ceramics Division 10 West 35th Street Chicago, IL 60616	1	Materials Science Lab.	
Naval Ship R&D Center Washington, DC 20007	1	U. S. Army Aviation Material Laboratories Fort Eustis, VA 23604	1
Naval Ship R&D Center Annapolis Lab. (Code 287) Annapolis, MD 21402	1	Effects Technology, Inc. Attn: F. R. Tuler P. O. Box 30400 Santa Barbara, CA 93105	1

Naval Undersea R&D Center San Diego, CA 92117	1	Plastics Technical Evaluation Center Picatinny Arsenal Dover, NY 07801	1
Engineering Experiment Station Georgia Institute of Technology Atlanta, GA 30332	1	University of Dayton Library on Materials Research 300 College Park Avenue Dayton, OH 45409	1
Goodyear Aerospace Corporation Attn: G. Wintermute Litchfield Park, AZ 85340	1	University of Michigan Attn: F. G. Hammitt Dept. of Nuclear Engineering Ann Arbor, MI 48104	1
Pratt & Whitney Aircraft Div. United Aircraft Corporation Attn: C. C. Goodrich East Hartford, CT 06108	1	Olin Corporation Chemical Group New Haven, CT 06540	1
TRW Equipment Lab 23555 Euclid Avenue Cleveland, OH 44117	1	Aerospace Corporation Materials Laboratory P.O. Box 95085 Los Angeles, CA 90045	1
Aero-Electronic Technology Dept. Attn: George Tatnall Naval Air Development Center Warminster, PA 18974	1	Air Force Avionics Laboratory Wright Patterson AFB Dayton, OH 45433 Attn: AVTL	1
Vought Aeronautics Division Attn: A. E. Hohman, Jr. LTV Aerospace Corporation P.O. Box 5907 Dallas, TX 75222	1	U.S. Army Research Office Box CM, Duke Station Durham, NC 27706	1
Engineered Fabrics Division Goodyear Aerospace Corporation Akron, OH 44315	1	Applied Technology Division Avco Corporation Lowell Industrial Park Lowell, MA 01851	1
Bell Aerosystems Company Attn: N. E. Wahl Buffalo, NY 14240	1	Solar Division Attn: Dr. A. G. Metcalfe International Harvester Company 2200 Pacific Highway San Diego, CA 92112	1
Hydronautics, Incorporated Pindell School Road Howard County Laurel, MD 20810	1	Material Sciences Corporation 17777 Walton Road Blue Bell, PA 19422	1
Brunswick Corporation Marion, VA 24354	1		

University of Illinois Attn: Prof. H. T. Corten Dept. of Theoretical & Applied Mechs. Urbana, IL 61801	1	Dr. S. S. Sternstein Rensselaer Polytechnic Institute 110 8th Street Troy, NY 12181	1
Naval Ship Engineering Center Attn: Code 6101E Washington, DC 20361	1	Prof. R. Doremus Rensselaer Polytechnic Institute 110 8th Street Troy, NY 12181	1
Westinghouse Research Labs. Attn: R. Bratton Beulah Road Pittsburgh, PA 15235	1	Prof. M. Goldstein Belfer Graduate School Yeshiva University 500 W. 185 Street New York, NY 10033	1
E. I. duPont deNemours & Company Attn: C. Zweben, Bldg. 262 Textile Fibers Dept. Carothers Research Lab Experimental Station Wilmington, DE 19898	1	John D. Ferry Department of Chemistry University of Wisconsin Madison, WI 53706	1
NTDSC Southwest Research Institute P. O. Drawer 28510 San Antonio, TX 78284	1	Library National Bureau of Standards Washington, DC 20234	1
Texas A&M University Attn: Prof. J. L. Rand Aerospace Engineering Dept. College Station, TX 77843	1	Prof. J. H. Gibbs Metcalf Chem. Lab. Brown University Providence, RI 02912	1
Dr. George C. Chang Advanced Physical Methods Branch Division of Energy Storage Systems Office of Conservation U. S. Energy Research and Development Administrations Washington, DC 20545	1	Polymer Research Institute Univ. of Massachusetts Amherst, MA 01002	1
Prof. D. Uhlmann Massachusetts Institute of Technology Cambridge, MA 02139	1	Dr. T. Alfrey, Jr. Polymer Research Lab. Dow Chemical Company Midland, MI 48640	1
		Prof. N. Brown Metallurgy Dept. Univ. of Pennsylvania Philadelphia, PA 19104	1

D-4

Dr. S. Krimm
Univ. of Michigan
Ann Arbor, MI 48104

R. S. Marvin
National Bureau of Standards
Washington, DC 20234

1 Prof. John F. Fellers 1
Polymer Science & Engineering
Program
419 Dougherty Engineering Building
1 University of Tennessee
Knoxville, TN 37916